

Electromagnetic induction in thin sheets: integral equations and model studies in two dimensions

U. Schmucker

Geophysikalisches Institut, Universität Göttingen, 37075 Göttingen, Germany

Accepted 1994 August 25. Received 1994 August 1; in original form 1993 November 25

SUMMARY

The model consists of a thin sheet of variable conductance in one horizontal direction above a conducting substructure of lateral uniformity. Transition anomalies are permitted, i.e. the anomalous range of varying conductance may be bounded by uniform half sheets of different conductances. For *E*-polarization the inducing external source field may be non-uniform. Two complementary integral equations are derived in the frequency–distance domain, to find the anomalous electric field or alternatively to find the anomalous sheet current density for each polarization. The equations involve two sets of response functions for the normal structure outside the anomalous range. A first set generates for a given source field at ground level the internal magnetic field by induction and the normal electric field which serves as an input function for the derivation of the anomalous field. A second set accounts for the inductive coupling of the anomalous fields in sheet and substructure. Various tests are performed: for the compatibility of complementary solutions, for the correct asymptotic behaviour at infinity in the horizontal direction, and for the accuracy of numerical integrations as controlled by the grid-point spacing. The numerical solutions are also tested against analytical solutions and against numerical solutions by other methods, in particular with regard to the validity of the thin-sheet approximation. A comparison with results from integral equations, which involve conventional Green's functions, reveals in the case of *B*-polarization complications where a strong influx of currents exists from the substructure into the thin sheet. A source transfer function is introduced which allows the extension of the response function concept to induction by non-uniform sources. Two types are studied: a stationary jet field source and a travelling *Sq* source above a sedimentary basin and a coastline. Resulting magnetotelluric and geomagnetic deep sounding responses are compared with the respective responses, when the inducing field is quasi-uniform.

Key words: conductance of oceans and sediments, electrojet and *Sq* induction, quasi-uniform and non-uniform sources, 2-D thin-sheet induction.

1 INTRODUCTION

Thin sheets and shells are convenient approximations to simplify model calculations in electromagnetic induction studies of the Earth's conductivity. At sufficiently low frequency they represent oceans and well-conducting geological strata on land which overlay more resistive crystalline rocks. This contribution extends earlier work on the subject (Schmucker 1970, 1971), with special emphasis on induction by non-uniform fields. If their spatial dimensions are of the same order as their penetration depth into the conducting Earth, then the source geometry cannot be ignored in the interpretation of data by models.

Practical applications arise in the vicinity of auroral and dip-equatorial jets, when geomagnetic or magnetotelluric studies of the deep conductivity structure are performed with variations in the period range of hours. The smallness of source dimension and penetration depth in comparison with the Earth's radius allows the use of plane conductivity models in rectangular (*x, y, z*) coordinates, *z* positive down. The thin sheet, assumed to be of infinitely small thickness, occupies the *z* = 0 plane, with its upper surface at *z* = -0 and its lower surface at *z* = +0. The air space above is non-conducting up to the height of the primary source region, the space below is conducting and carries together with the thin-sheet the secondary sources by induction.

Lateral changes of conductivity will be confined to the thin sheet and here restricted to one horizontal direction. Following the convention for 2-D induction problems, x will be the strike direction of the structure. The depth-integrated conductivity of the sheet, henceforth referred to as *conductance* $\tau(y)$, will be dependent on y within a bounded range and constant outside. The time-harmonic primary source has $\exp(+i\omega t)$ as time factor and is in the tangential electric mode. Its electric field is linearly polarized either in the x -direction (E -polarization) or in the y -direction (B -polarization).

Electromagnetic modelling, using the thin sheet or thin-shell approximation, has progressed beyond the restrictions imposed here. Thin sheets with a variable conductance in both horizontal directions are now part of standard modelling techniques, thanks to the work by Vasseur & Weidelt (1977) and Yegorov *et al.* (1983), among others. The usual limitation of such models is that the anomalous domain has to merge into the same normal structure in all directions. It has been overcome in the work of Dawson & Weaver (1979) and extended by McKirdy, Weaver & Dawson (1985). Spherical shells of variable conductance, enclosing a radially symmetric conducting Earth, have been studied extensively by Hobbs & Brignall (1976), Hewson-Browne (1978), and Zinger & Fainberg (1980). Their work has been summarized most recently by Fainberg, Kuvshinov & Singer (1990).

Furthermore, it is not difficult to combine thin sheets or shells with a multidimensional substructure or to form stacks of thin sheets simulating such structures (Ranganayaki & Madden 1980). Finally, methods have been developed to extend the original Price approximation by allowing the electric field to be slightly different at the top and bottom of the thin sheet (Dmitriev 1969). Berdichevsky & Zhdanov (1984) present a summarizing overview on the subject in Chapter 2 of their treatise.

In practical situations, however, there are not always enough observations to specify adequately the source field structure as well as the internal conductivity structure for such advanced models. In such cases the following simplified modelling concept may still be useful and illuminating, also in view of its more elementary theoretical foundations. An example is the accompanying contribution by Ogunade (1995).

2 BASIC MODELLING CONCEPT

The treatment follows Price's (1949) original concept that the tangential electric field within the thin sheet is sufficiently uniform to approximate it by a depth-independent vector \mathbf{E}_h between its outer and inner surfaces. Hence, Ohm's law to derive the depth-integrated current density, hereafter termed *sheet current density* \mathbf{j} , is $\mathbf{j} = \tau \mathbf{E}_h$.

The first field equation, when at sufficiently low frequencies displacement currents can be ignored in conducting matter, is $\text{curl } \mathbf{B} = \mu_0 \mathbf{j}$ with \mathbf{B} as magnetic flux density and \mathbf{j} as current density. Integration over the thickness of the thin sheet yields that the difference of the tangential components of \mathbf{B} on the upper (-) and lower (+) surface is given by the depth-integrated current flowing in the sheet:

$$B_y^- - B_y^+ = \mu_0 j_x = \mu_0 \tau E_x \tag{1}$$

for E -polarization and

$$B_x^+ - B_x^- = \mu_0 j_y = \mu_0 \tau E_y \tag{2}$$

for B -polarization. The vertical magnetic field B_z (in the case of E -polarization) is again depth-independent as readily inferred from the continuity of \mathbf{E} in $\text{rot}_z \mathbf{E} = -i\omega B_z$. The anomalous vertical electric field E_{az} (in the case of B -polarization) needs special consideration.

Magnetic and electric fields which appear in these Price equations will be connected by conditions at infinity. The downward diffusing total field in the lower half-space must vanish for $z \rightarrow +\infty$, and the upward propagating secondary field must vanish for $z \rightarrow -\infty$. Satisfying these conditions solves the thin-sheet induction problem. Both fields will be split into normal and anomalous parts in the sense that the conductance to the left of the anomalous range defines the conductance τ_n of the normal structure (Fig. 1). Transition anomalies are permitted, i.e. the conductance τ_N to the right of that range may be different from τ_n . The subscript n identifies the normal field for induction in the normal structure. Its components in the $z = 0$ plane are

$$E_{nx}, B_{nx}^+, B_{nx}^-, B_{nz}$$

for E -polarization, assumed to be complex-valued functions of frequency ω and distance y , and

$$B_{ny}^+, B_{ny}^-, E_{ny}$$

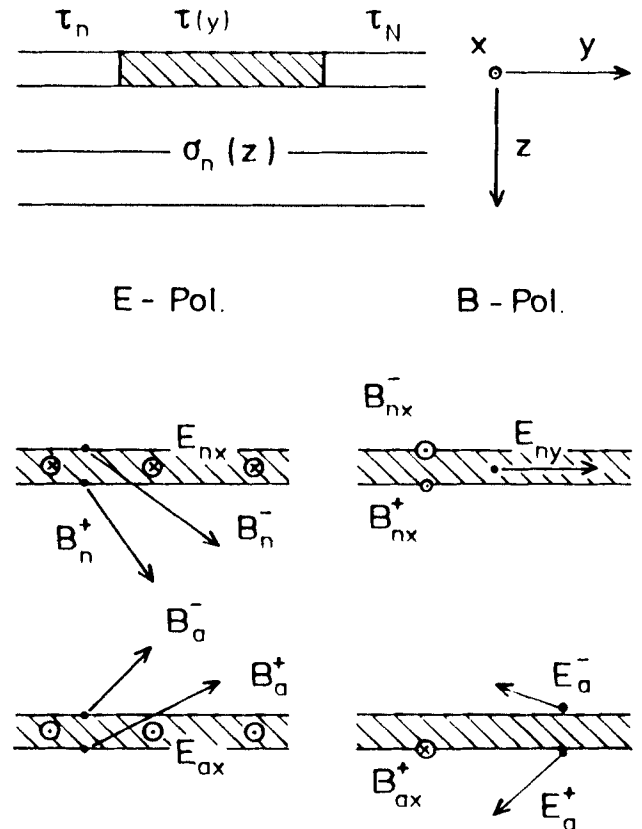


Figure 1. (Top) the thin-sheet model; (below) normal and anomalous field vectors, assuming a non-uniform source in E -polarization and a quasi-uniform source in B -polarization. Note the same vertical magnetic components at the upper and lower surfaces for E -polarization, but different vertical electric components for B -polarization.

for B -polarization, assumed to be only functions of frequency for reasons given later.

The subscript a identifies the anomalous field which arises from the variable conductance in the anomalous range: a *tangential electric* field for E -polarization and a *tangential magnetic* field for B -polarization.

Both modes obey the field equations $\text{rot } \mathbf{B}_a = \mu_0 \mathbf{t}_a$ and $\text{rot } \mathbf{E}_a = -i\omega \mathbf{B}_a$, yielding with $\partial/\partial x = 0$

$$-\frac{\partial B_{ax}}{\partial y} = \mu_0 \sigma E_{az} \quad (3)$$

for B -polarization (in the quasi-stationary approximation) and

$$\frac{\partial E_{ax}}{\partial y} = i\omega B_{az} \quad (4)$$

for E -polarization. The sum of normal and anomalous fields is the total field without subscript.

Equation (3) implies that B_{ax} is constant or zero in the non-conducting free space above the thin sheet and that no current leaves the thin sheet through its upper surface, even though E_{az} here is not necessarily zero. Since \mathbf{E}_a for B -polarization above the thin sheet is a potential field of accumulated charges on $z=0$, a Hilbert transformation connects E_{az} with E_{ay} at any level $z < 0$, e.g. $E_{az}(y, -0) = K(y) * E_{ay}(y, 0)$ with the notation of eq. (15). But there is no need to consider E_{az}^- any further.

The remaining anomalous field components in the $z=0$ plane are

$$E_{ax}, B_{ay}^+, B_{ay}^-, B_{az}$$

for E -polarization and, with the condition $B_{ax}^- = 0$,

$$B_{ax}^+, E_{ay}^+, E_{az}^+$$

for B -polarization, all being functions of ω and y (Fig. 1).

A final note on the validity range of the thin-sheet concept follows. A conducting layer of thickness d and conductivity σ , underlain by a laterally uniform conductive substructure, may be regarded as *thin* in the above sense, if at the considered frequency ω and wavenumber k two conditions are met: first, the layer must be thin enough that d is much smaller than the skin depth $p = \sqrt{2/\omega\mu_0\sigma}$, when $kp \ll 1$, or $|K|^{-1}$ in general with $K = \sqrt{2i/p^2 + k^2}$ as the vertical wavenumber; second, the substructure must be resistive enough that the penetration depth into it is much larger than d .

These conditions are readily inferred from the diffusion formula of layered structures, expressing the downward attenuation of a tangential electric field by conducting matter. Let E^- denote the field at the upper boundary of the layer, and E^+ the attenuated field at its lower boundary. Then (Schmucker 1970; eqs 5.43 and 5.47)

$$E^+ = \frac{KC^+}{KC^+ \cosh \alpha + \sinh \alpha} E^-,$$

where $\alpha = Kd$; C^+ , as a measure of the penetration depth, is the C -response of the substructure below the lower boundary, defining in $E_x^+ = i\omega C^+ B_y^+$ the impedance relation on this boundary.

The first condition $d \ll p$ ensures that $\cosh \alpha \approx 1$ and $\sinh \alpha \approx \alpha$, the second condition $|C^+| \gg d$ that $|KC^+| \gg |\alpha|$,

which yields $E^+ \approx E^-$. Since $|E|$ decreases monotonically downward, the required quasi-uniformity of the tangential electric field within the layer is established. The arguments can be generalized to non-uniform layers, provided that lateral field changes on its boundaries are sufficiently smooth.

3 ELECTROMAGNETIC RESPONSE FUNCTIONS FOR THE NORMAL STRUCTURE

The equations, which will be formulated for the anomalous field in the next section, involve certain response functions in reference to the normal structure. They are complex-valued functions of frequency ω and distance y , defined as Fourier transforms of corresponding response functions in the frequency-wavenumber domain, and will be related to conventional Green's functions.

Let $Z^-(\omega, k) = i\omega\mu_0 C^-(\omega, k)$, defined as a function of ω and wavenumber k , be the impedance at $z = -0$ of the normal structure for tangential electric fields. The C -response function introduced in this manner will be used exclusively hereafter. It can be derived by standard methods, for example with Wait's algorithm for layered structures. Let $\hat{\mathbf{E}}_n(\omega, k_y)$, $\hat{\mathbf{B}}_n^-(\omega, k_y)$ be Fourier transforms of the normal field vectors $\mathbf{E}_n(\omega, y)$, $\mathbf{B}_n^-(\omega, y)$, with $\exp[i(k_y y + \omega t)]$ as the common time-distance factor and $k = |k_y|$. Their relations in the (ω, k) domain are

$$\hat{E}_{nx} = i\omega C^- \hat{B}_{ny} \quad \text{and} \quad \hat{E}_{ny} = -i\omega C^- \hat{B}_{nx}. \quad (5)$$

The convention used here for Fourier transforms is

$$\hat{f}(k_y) = \int_{-\infty}^{+\infty} f(y) \exp(ik_y y) dy,$$

$$f(y) = \frac{1}{2\pi} \int_{-\infty}^{+\infty} \hat{f}(k_y) \exp(-ik_y y) dk_y.$$

Let the normal magnetic field vector for E -polarization at $z = -0$ be split into an external primary part \mathbf{B}_e and an internal secondary part \mathbf{B}_i , the latter from induced currents in the normal structure. The Q -response, given by (Schmucker 1970, eq. 5.37)

$$Q(\omega, k) = \frac{1 - kC^-(\omega, k)}{1 + kC^-(\omega, k)}, \quad (6)$$

defines then the internal field components in terms of those of the external field:

$$\hat{B}_{iy} = Q\hat{B}_{ey} \quad \text{and} \quad \hat{B}_{iz} = -Q\hat{B}_{ez}. \quad (7)$$

Combining eqs (5) to (7) connects the normal electric field within the thin sheet to the external source field:

$$\hat{E}_{nx} = i\omega C^-(1 + Q)\hat{B}_{ey} = i\omega \frac{2C^-}{1 + kC^-} \hat{B}_{ey}. \quad (8)$$

Now a Fourier transformation back into the (ω, y) domain is performed with eqs (7) and (8). It leads to

$$B_{iy} = P * B_{ey}, \quad B_{iz} = -P * B_{ez} \quad (9)$$

and

$$E_{ny} = 2i\omega S^- * B_{ey} \quad (10)$$

with P and S^- representing the Fourier transforms of Q and $C^-/(1+kC^-)$, respectively. The sign $*$ implies convolution, e.g. the expression $B_{iy} = P * B_{ey}$ stands for

$$B_{iy}(\omega, y) = \int_{-\infty}^{+\infty} P(\omega, y') B_{ey}(\omega, y - y') dy'.$$

Since Q and C depend on k and thus are even functions of k_y , they can be written as one-sided cosine transforms:

$$P(\omega, y) = \frac{1}{\pi} \int_0^{\infty} Q(\omega, k) \cos ky dk, \quad (11)$$

$$S^-(\omega, y) = \frac{1}{\pi} \int_0^{\infty} \frac{C^-(\omega, k)}{1 + kC^-(\omega, k)} \cos ky dk. \quad (12)$$

Once these response functions in the (ω, y) domain have been found for a given normal structure, the normal internal magnetic and normal electric fields follow for any specified source field at ground level $z = -0$ from eqs (9) and (10).

Three additional notes:

(1) The physical implications of P and S^- can be visualized as follows: let B_{ey} be the field of a narrow sheet current of width ε just above the thin sheet at point y_0 , flowing with density j_{ex} or total strength εj_{ex} in the negative x -direction. Then for a point source of infinitely small width

$$B_{ey}(y, 0) = -\frac{1}{2} \mu_0 j_{ex} \delta(y - y_0).$$

Insertion into eqs (9) and (10) identifies $P(\omega, y)$ as the magnetic field of currents, which a point source at $z_0 = -0$ induces in the normal structure, and $i\omega\mu_0 S^-(\omega, y)$ as its electric field, both for field points at $z = 0$. In this way S^- can be regarded as a Green's function for the specified levels of source and field points, while P involves a differentiation of this function with respect to z .

(2) The inverse transformation of eqs (11) and (12) for wavenumber $k = 0$ shows that

$$\int_{-\infty}^{+\infty} P(\omega, y) dy = Q(\omega, 0) = 1 \quad (13)$$

and that

$$\int_{-\infty}^{+\infty} S^-(\omega, y) dy = C^-(\omega, 0). \quad (14)$$

(3) The external magnetic field in the lower air space is a potential field in the quasi-stationary approximation. Hence its components are Hilbert transforms of each other (Kertz 1954). With the correct sign for fields of external origin they read at ground level

$$B_{ey} = +K * B_{ez} \quad \text{and} \quad B_{ez} = -K * B_{ey} \quad (15)$$

with the convolution kernel $K(y) = 1/\pi y$ as the sine transform of $-ik_y/k$ (cf. eq. (27)).

The remaining response functions are related to the

anomalous field and its diffusion into the substructure below the thin sheet. Let $C^+(\omega, k)$ be the C -response at the top of this substructure and let

$$\hat{E}_{ax} = i\omega C_{TE}^+ \hat{B}_{ay}^+, \quad \hat{B}_{ax}^+ = -\mu_0 \sigma^+ C_{TM}^+ \hat{E}_{ay} \quad (16)$$

be the respective impedance and admittance relations at $z = +0$. A distinction has to be made between the C -response of the tangential electric anomalous field for E -polarization (TE) and the C -response of the tangential magnetic anomalous field for B -polarization (TM), σ^+ denoting the conductivity at the very top of the substructure. In writing these relations the definitions $C_{TE}^+ = -\hat{E}_{ax}/\hat{E}'_{ax}$ and $C_{TM}^+ = -\hat{B}_{ax}/\hat{B}'_{ax}$ are used with $\hat{E}'_{ax} = -i\omega\hat{B}_{ay}$ and $\hat{B}'_{ax} = +\mu_0\sigma^+\hat{E}_{ay}$ from the quoted field equations for the anomalous field, the prime denoting derivatives with respect to z .

The vertical components of the respective poloidal modes, expressed in terms of their tangential fields, are:

$$\hat{B}_{az} = ik_y C_{TE}^+ \hat{B}_{ay}^+, \quad \hat{E}_{az}^+ = ik_y C_{TM}^+ \hat{E}_{ay}, \quad (17)$$

as seen from eqs (16) and (20) below. Note that E_{az}^+ in contrast to B_{az}^- differs from E_{az}^- , as already discussed, which is the vertical component of a potential field and given by $-i(k_y/k)\hat{E}_{ay}$ in analogy to eq. (18).

Finally, the internal origin of the anomalous magnetic potential has to be observed, yielding in analogy to the external magnetic field, but with reversed signs,

$$B_{ay} = -K * B_{az} \quad \text{and} \quad B_{az} = +K * B_{ay}$$

or

$$\hat{B}_{ay}^- = +i(k_y/k)\hat{B}_{az} \quad \text{and} \quad \hat{B}_{az}^- = -i(k_y/k)\hat{B}_{ay}^- \quad (18)$$

These relations are now combined with the field equations for the anomalous field in the (ω, k) domain. The depth-integrated first field equations for E - and B -polarization are

$$\hat{B}_{ay} - \hat{B}'_{ay} = \mu_0 \hat{j}_{ax} \quad \text{and} \quad \hat{B}_{ax} = \mu_0 \hat{j}_{ay}, \quad (19)$$

observing that the anomalous magnetic field B_{ax} is zero, while it follows from eqs (3) and (4) that

$$k_y \hat{E}_{ax} = \omega \hat{B}_{az} \quad \text{and} \quad -\mu_0 \sigma^+ \hat{E}_{az}^+ = ik_y \hat{B}_{ax}^+ \quad (20)$$

Expressing \hat{B}_{ay} in eq. (19) for E -polarization in terms of \hat{B}_{az} , using eqs (17) and (18), and then replacing \hat{B}_{az} by $(k_y/\omega)\hat{E}_{ax}$, we can connect the anomalous sheet current density and the anomalous electric field as follows:

$$\hat{E}_{ax} = -i\omega\mu_0 \frac{C_{TE}^+}{1 + kC_{TE}^+} \hat{j}_{ax}. \quad (21)$$

The Fourier transforms of eqs (16) and (17) for B -polarization and eqs (17), (18) and (21) for E -polarization into the (ω, y) domain are

$$B_{ax}^+ = -\mu_0 \sigma^+ N * E_{ay}, \quad E_{ay} = L_{TM} * E_{az}^+, \quad (22)$$

$$B_{ay}^+ = L_{TE} * B_{az}, \quad B_{az} = -K * B_{ay}, \quad (23)$$

$$E_{ax} = -i\omega\mu_0 S^+ * j_{ax} \quad (24)$$

with response functions introduced as follows:

$$N(\omega, y) = \frac{1}{\pi} \int_0^{\infty} C_{\text{TM}}^+(\omega, k) \cos ky \, dk, \quad (25)$$

$$L(\omega, y) = \frac{1}{\pi} \int_0^{\infty} [kC^+(\omega, k)]^{-1} \sin ky \, dk, \quad (26)$$

$$K(y) = \lim_{\epsilon \rightarrow +0} \frac{1}{\pi} \int_0^{\infty} \exp(-k\epsilon) \sin ky \, dk = \frac{1}{\pi y}, \quad (27)$$

$$S^+(\omega, y) = \frac{1}{\pi} \int_0^{\infty} \frac{C_{\text{TE}}^+(\omega, k)}{1 + kC_{\text{TE}}^+(\omega, k)} \cos ky \, dk. \quad (28)$$

In eq. (26) C_{TE}^+ and C_{TM}^+ are used for the responses L_{TE} and L_{TM} , respectively. In deriving K and L by sine transforms it has been noted that $\text{sgn}(k_y)$ and $k_y C^+$ are odd functions of k_y . Again

$$\int_{-\infty}^{+\infty} N(\omega, y) \, dy = C_{\text{TM}}^+(\omega, 0), \quad (29)$$

$$\int_{-\infty}^{+\infty} S^+(\omega, y) \, dy = C_{\text{TE}}^+(\omega, 0)$$

in correspondence to eq. (14). In the case of layered substructures the C^+ responses can be derived with the same algorithm for both modes, when in the TE case the continuity of the impedance and in the TM case the continuity of the admittance, as expressed by eq. (16), are observed (*cf.* Schmucker 1971, Appendix A).

In the numerical evaluation of the convolution integrals the following characteristics of the response functions have to be observed: for $y \rightarrow \pm\infty$ all responses except L approach zero on a distance scale which is given by the zero-wavenumber response $C^+(\omega, 0)$. This response also determines the finite limiting value of L , which is

$$L(\omega, y) \rightarrow [2C^+(\omega, 0)]^{-1} \quad \text{for } y \rightarrow \infty. \quad (30)$$

For $y \rightarrow 0$ all responses, except P , become singular, with logarithmic singularities for the even responses S and N , and $1/y$ singularities for the odd responses K and L . They can be overcome by expressing the field which is to be convolved as a Taylor series in the vicinity of the singularities, and by integrating term by term (*cf.* Schmucker 1971, Appendix B).

Similarly, the characteristics of the C -response have to be observed, when deriving the (ω, y) -domain responses by Fourier transformations. For $k \rightarrow \infty$ the C -response of any layered structure approaches $1/k$ and for $k \rightarrow 0$ it merges into the zero wavenumber response with $\partial C/\partial k = 0$. Hence, the required cosine transforms for P , N and S are readily performed, making use of tabulated cosine integrals for $k \geq k_{\text{max}}$ and $C^+ \approx 1/k$. The numerical evaluation of the sine transform for the derivation of L , however, has to be modified to avoid problems when k becomes large. This is done by separating the Hilbert transform kernel, i.e. by setting $L = K + L'$. The integrand of the sine transform for L' then becomes $(1/kC^+ - 1)$, which vanishes for $k \rightarrow \infty$.

In a few special cases the transformations can be carried

out analytically. For a uniform substructure of conductivity σ it follows from $C^+ = 1/\sqrt{k^2 + i\omega\mu_0\sigma}$ that

$$N(\omega, y) = \frac{1}{\pi} K_0(\sqrt{i\mu_0\sigma} |y|), \quad (31)$$

with K_0 as a modified Bessel function of the second kind and zero order. For a non-conducting substructure down to depth h , where it becomes perfectly conducting, C_{TE}^+ equals $\tanh(kh)/k$, from which follows

$$L_{\text{TE}} = [2h \tanh(\pi u)]^{-1} \quad \text{and} \quad S^+ = [2\pi h(1 + u^2)]^{-1} \quad (32)$$

with $u = 2h/y$. No anomalous field in B -polarization exists because in this model the thin sheet is also insulated from below and currents can neither enter nor leave the sheet.

4 INTEGRAL EQUATIONS FOR THE ANOMALOUS ELECTRIC FIELDS AND CURRENTS

Starting with E -polarization, the relevant Price equation is

$$B_{\text{av}}^- - B_{\text{av}}^+ = \mu_0 j_{\text{av}} \quad (33)$$

and the depth-integrated Ohm's law is

$$j_{\text{av}} = \tau_a E_{\text{av}} + \tau E_{\text{av}} \quad (34)$$

with $\tau_a = \tau - \tau_n$ and $j_{\text{av}} = j_x^+ - j_{\text{nx}}^-$, $j_{\text{nx}}^- = \tau_n E_{\text{nx}}^-$. For a non-uniform source the normal electric field E_{nx} depends on y and has to be inferred from eq. (10) for a specified external source field at ground level. The normal magnetic field with the components B_{nx} and B_{nz} follows from eq. (9) as the sum of external and internal parts.

If the source field is quasi-uniform in the sense that its penetration depth is small in comparison with its lateral spatial dimensions, then eqs (13) and (14) imply that the normal horizontal field B_{ny} is just twice the external source field, while B_{nz} is zero, and that $E_{\text{nx}} = i\omega C^+(\omega, 0) B_{\text{ny}}$ which is the Cagniard-Tikhonov approximation of magnetotellurics.

Hence, $E_{\text{nx}}(\omega, y)$ in eq. (34) can be assumed to be known. Inserting E_{av} from eq. (24) leads to an integral equation for the anomalous current density:

$$i\omega\mu_0 \tau S^+ * j_{\text{av}} = \tau_a E_{\text{av}} - j_{\text{av}} \quad (35)$$

Alternatively, replacement of B_{av}^- and B_{av}^+ in eq. (33) by B_{az} according to eq. (23) gives for the anomalous electric field, when B_{az} is substituted with eq. (4):

$$-(K + L_{\text{TE}}) * \frac{\partial E_{\text{av}}}{\partial y} = i\omega\mu_0 (\tau_a E_{\text{av}} + \tau E_{\text{av}}). \quad (36)$$

Integration by parts, as discussed in the following section, converts the convolution integral on the left into a convolution of E_{av} with the derivatives of K and L with respect to y and thus transforms eq. (36) into an integral equation for E_{av} .

Once j_{av} or E_{av} have been found, the undetermined quantity can be derived with Ohm's law. Differentiating E_{av} yields B_{az} and a subsequent Hilbert transformation gives $B_{\text{ay}}^- = -K * B_{\text{az}}$. Adding these anomalous fields to the normal field yields the total magnetic field \mathbf{B} on the upper surface and in $E_x = E_{\text{nx}} + E_{\text{av}}$ the total electric field. If the magnetic field at the lower surface is sought, for instance for

a comparison with magnetic sea-floor observations, B_v^+ is readily inferred from Price's eq. (33).

The B -polarization case can be treated in a corresponding way. To keep the induction problem 2-D, the source must be quasi-uniform in the sense described above, i.e. $E_{ny} = -i\omega C(\omega, 0)B_{nx}$. Inserting B_{nx}^+ from eq. (22) into the form of the Price equation $B_{nx}^+ = \mu_0 j_{ay}$ relevant here, yields with the depth-integrated Ohm's law $j_{ay} = \tau_n E_{ny} + \tau E_{ay}$

$$-\sigma^+ N * E_{ay} = \tau_n E_{ny} + \tau E_{ay} \quad (37)$$

as a first integral equation for E_{ay} .

Equation (3) implies in conjunction with the Price equation that at $z = +0$, but already within the substructure,

$$\sigma^+ E_{az} = -\frac{\partial j_{ay}}{\partial y},$$

where E_{az}^+ accounts for the fact that in B -polarization induced currents enter and leave the thin sheet from below. Let E_{ay} in Ohm's law be replaced by $L_{TM} * E_{az}^+$ according to eq. (22), and E_{az}^+ by $\partial j_{ay}/\partial y$ according to the above relation. This gives in

$$\left(L_{TM} * \frac{\partial j_{ay}}{\partial y}\right) / \sigma^+ = (\tau_n E_{ny} - j_{ay}) / \tau \quad (38)$$

a second integral equation, now for j_{ay} . Again two alternative methods exist to solve the thin-sheet B -polarization modelling problem.

The accommodation of transition anomalies is readily seen. The integrals to be evaluated involve either derivatives of the anomalous field or current, which in any case disappear at great distance from the anomalous range or response functions which are readily evaluated with constant asymptotic fields and currents by virtue of eq. (29). It should be noted that eqs (36) and (37) can be written explicitly for τ_n and thus provide direct solutions of the 2-D thin-sheet inverse problem: to find its conductance from an observed electric field for a given normal structure (and source).

It will be interesting to add integral equations for the horizontal electric fields which evolve from Green's theorem. Their important distinctions are that (1) the integration is limited to the anomalous range $[-a, a]$ in y (which must be bounded), (2) the remaining anomalous field components can be derived also from integral equations, involving differentiated Green's functions with respect to fieldpoint coordinates, (3) the anomalous field outside the thin sheet is included. The E -polarization integral equation is

$$-i\omega\mu_0 \int_{-a}^{+a} \tau_n(y') E_x(y', 0) G_{TE}(y, z; y', 0) dy' = E_{ax}(y, z), \quad (39)$$

to be solved for $z = 0$ with G_{TE} as the cosine transform of

$$\frac{C_{TE}^+}{1 + kC_{TE}^+ + i\omega\mu_0\tau_n C_{TE}^+}. \quad (40)$$

Except for an additional source layer term in the denominator it resembles the transform of S^+ in eq. (35).

Furthermore, G_{TE} is identical with the response function S of Section 3. From

$$\begin{aligned} B_{ny}^- - B_{ny}^+ &= \mu_0 \tau_n E_{ny} \\ &= i\omega\mu_0 \tau_n C_{TE}^+ B_{ny} = i\omega\mu_0 \tau_n C_{TE}^+ B_{ny}^+ \end{aligned}$$

it follows readily that

$$i\omega\mu_0 \tau_n C_{TE}^+ = C_{TE}^+ / C_{TE}^- - 1$$

which when inserted into eq. (40) reveals G_{TE} as the cosine transform of $C_{TE}^+ / (1 + kC_{TE}^+)$ in accordance with the definition of S^+ in eq. (12).

The B -polarization integral equation for $z \geq +0$ is

$$\int_{-a}^{+a} \tau_n(y') E_v(y', 0) G_{TM}(y, z; y', 0) dy' = \tau_n B_{ax}(y, z) / \mu_0, \quad (41)$$

to be solved for $z = +0$ with G_{TM} as the cosine transform of

$$\frac{\sigma^+ C_{TM}^+}{1 + \sigma^+ C_{TM}^+ / \tau_n} \quad (42)$$

reflecting the transform of $\sigma^+ N$ in eq. (37). Let $R = 1/\tau$ denote the reciprocal thin-sheet conductance and $R_a = R - 1/\tau_n$ its anomalous part. Then with $j_{ay} = B_{ax}^+ / \mu_0$ and $\tau_n = -R_a \tau_n \tau$ eq. (41) is conveniently reformulated as an integral equation for the sheet current density $j_y = \tau E_y$ which in contrast to E_y is continuous in y :

$$- \int_{-a}^{+a} R_a(y') j_y(y') G_{TM}(y, +0; y, 0) dy' = j_{ay}. \quad (43)$$

The case when a strong influx of currents from a well-conducting substructure occurs deserves special attention. If in that case the inequality $|C_{TM}^+ \sigma^+| \gg \tau_n$ holds for any wavenumber, for which C_{TM}^+ has not yet reached its asymptotic value $1/k$, the Green's function approaches

$$\tau_n \frac{1}{\pi} \int_0^\infty \frac{1}{\tau_n k / \sigma^+ + 1} \cos[k(y' - y)] dk = \sigma^+ g(\alpha)$$

as a limiting static value with

$$g(\alpha) = -\cos \alpha Ci(\alpha) - \sin \alpha \left[\frac{\pi}{2} - Si(\alpha) \right]$$

and $\alpha = |y' - y| \sigma^+ / \tau_n$. Here $Ci(\alpha)$ and $Si(\alpha)$ denote the cosine and sine integrals. Because $g(\alpha)$ varies then on a distance scale given by τ_n / σ^+ , the numerical evaluation of integral equation (43) may require a much finer grid spacing than the evaluation of eqs (37) and (38). The distance scale of their kernel function is solely determined by C_{TM}^+ for $k = 0$, assumed to be large against τ_n / σ^+ .

In conclusion, it will be shown how the last two integral equations, based on Green's functions G_{TE} and G_{TM} in their conventional definition for the *total* normal structure, connect to those derived earlier in this section which use the

response functions S^+ and N in reference to the substructure alone. The demonstration will be carried out in the wavenumber domain with

$$\hat{G}_{TE} = \frac{C_{TE}^+}{1 + kC_{TE}^+ + i\omega\mu_0\tau_n C_{TE}^+}$$

and

$$\hat{G}_{TM} = \frac{\sigma^+ C_{TM}^+}{1 + \sigma^+ C_{TM}^+ / \tau_n}$$

as the cosine transforms of G_{TE} and G_{TM} .

Multiply in the case of E -polarization eq. (21) with $(1 + kC_{TE}^+)$ and replace \hat{j}_{ay} by $\tau_n \hat{E}_{ax} + \hat{\tau}_a * \hat{E}_x$ according to Ohm's law; $\hat{\tau}_a(k)$ denotes the Fourier transform of $\tau_a(y)$. This gives

$$(1 + kC_{TE}^+ + i\omega\mu_0\tau_n C_{TE}^+) \hat{E}_{ax} = -i\omega\mu_0 C_{TE}^+ \hat{\tau}_a * \hat{E}_x$$

or, with the notation from above,

$$\hat{E}_{ax} = -i\omega\mu_0 \hat{G}_{TE} \hat{\tau}_a * \hat{E}_x$$

which is the Fourier transform of the first integral equation (39). Rewrite in the same manner eq. (16) for B -polarization with $\hat{B}_{ax}^+ = \mu_0 \hat{j}_{ay}$ and $\hat{E}_{ax} = R_n \hat{j}_{ay} + \hat{R}_a * \hat{j}_y$, when $R_n = 1/\tau_n$, yielding

$$(1 + \sigma^+ C_{TM}^+ R_n) \hat{j}_{ay} = -\sigma^+ C_{TM}^+ \hat{R}_a * \hat{j}_y$$

and thereby in

$$\hat{j}_{ay} = -\hat{G}_{TM} \hat{R}_a * \hat{j}_y$$

the Fourier transform of the second integral equation (43).

5 NUMERICAL SOLUTION OF THE INTEGRAL EQUATIONS

Anomalous field values are calculated for a sequence of N grid points along the y -axis, extending beyond the anomalous range into adjacent sections of constant conductance. These normal sections must be wide enough that the numerical solutions come sufficiently close to their respective limiting values at infinity. As a rule this requires a width of several penetration depths into the substructure, taking as a measure for this depth the real part of the zero-wavenumber C^+ -response in the relevant mode. The conductance within the anomalous range is assumed to be piecewise constant between grid points and the mean of adjacent sections is assigned to the grid points themselves: the arithmetic mean for E -polarization and the harmonic mean for B -polarization. This implies a certain smoothing of the numerical solutions.

The integrals are approximated by finite sums and the trapezoidal rule is used except for a range of one grid-point spacing to either side of the singularity of the convolution kernels. Within this range the integrals are evaluated analytically with a Taylor series expansion of the field, as discussed in Section 3 and below. The distance h between

grid points should be small enough that even in the best conducting section the dimensionless parameter

$$\eta_h = \omega\mu_0\tau h$$

is less than unity. For a thin sheet of thickness d and conductivity σ this parameter measures the cross-section dh of the numerical solution in relation to the squared skin depth $p^2 = 2/\omega\mu_0\sigma$. Because the response functions involved vary on a distance scale determined by the C -response of the substructure, a second independent condition requires that the grid-point spacing is sufficiently small to yield $h \ll |C^+(\omega, 0)|$.

The result is a system of N linear equations for the anomalous electric field and current at the chosen grid points. Because of the rapid decrease of the response functions with increasing distance from their singular points the matrix of coefficients is band-structured. Hence, rather than using a direct solution it can be more efficient to use approximate solutions, by limiting the number of off-diagonals. This is done by setting the responses formally to zero beyond a certain distance from the singular points. The more convenient solution with a band-shaped matrix gives preliminary field values, from which the omitted portions of the convolution integrals are calculated. Adding these portions to the knowns of the integral equations leads to modified right-hand sides of the N equations which are solved again. The iterative process is repeated until it converges. If it does not converge sufficiently fast within, say, 10 iterations, the number of off-diagonals must be increased.

The required convolutions with derivatives of the anomalous field and current in eqs (36) and (38) are performed as follows: in the vicinity of the $1/y$ singularities of K and L these derivatives are developed into Taylor series, preferably to high order, with a term-by-term integration. Outside this vicinity the convolution integrals are integrated by parts, leading to a convolution of the anomalous fields and currents themselves with the derivatives of K and L . This has the advantage that $\partial K/\partial y$ and $\partial L/\partial y$ diminish even more rapidly than K and L and that numerical differentiations of E_{ax} or j_{ay} are avoided altogether (*cf.* Schmucker 1986, pp. 40–43).

Special precautions are needed, if in the case of transition anomalies and quasi-uniform sources the L response is applied to a constant anomalous field. Clearly, the anomalous fields B_{ay}^+ for E -polarization and E_{ay} for B -polarization have to merge for $y \rightarrow +\infty$ into the constant differences of two normal solutions which are without vertical components. Hence, appropriate constants have to be added to the convolution integrals in eqs (22) and (23) as follows.

Let C_n^- be the zero-wavenumber C -response of the normal structure with τ_n as surface sheet conductance and C_N^- be the same response with τ_N , different from τ_n . Let E_{N_x} and $B_{N_x}^+$ denote the corresponding electric and magnetic fields at $y \rightarrow +\infty$, the latter at the lower surface. Then the anomalous fields B_{ay}^+ and E_{ay} have, for $y \rightarrow +\infty$, the limiting values

$$B_{ay}^+ = \frac{E_{N_x} - E_{nx}}{i\omega C_{TE}^+}$$

and

$$E_{oy} = -\frac{B_{Nz}^+ - B_{nz}^+}{\mu_0 \sigma^+ C_{TM}^+}$$

as seen from eq. (16), with

$$E_{Nz} - E_{nz} = i\omega(C_N - C_n) B_{ny}$$

and

$$B_{Nz}^+ - B_{nz}^+ = \mu_0(j_{Ny} - j_{ny}) = -i\omega\mu_0(\tau_N C_N^- - \tau_n C_n^-) B_{nz}^-$$

from the impedance and Price equation. For $y \rightarrow -\infty$, B_{ny} and E_{oy} approach zero by definition. Noting that the limiting value of L for $y \rightarrow \infty$ is $(2C^+)^{-1}$, the following expressions have to be added to the convolution integrals involving L (cf. Schmucker 1986, pp. 11–12):

$$-i\omega \frac{C_N - C_n}{2C_{TE}^+} B_{ny} \quad \text{to the left-hand side of eq. (36),}$$

$$-i\omega \frac{\tau_N C_N^- - \tau_n C_n^-}{2\sigma^+ C_{TM}^+} B_{nz}^- \quad \text{to the left-hand side of eq. (38).}$$

No correction is needed if a non-uniform source in E -polarization is stationary because it is assumed that its ground field does not extend beyond the range of the

numerical solution. Travelling non-uniform sources need special consideration (cf. Section 8).

6 TEST OF NUMERICAL SOLUTIONS

Figure 2 presents two test models. In the symmetrical model 1 the anomalous range is 300 km in width and has a uniform conductance of 1000 Siemens (S) for sediments against a normal value $\tau_n = 10$ S for basement rocks. The transition model 2 consists of two half-sheets, with $\tau_n = 10\,000$ S for oceans and $\tau_n = 10$ S for basement rocks on continents. The substructure is a uniform half-space of $100\,\Omega\text{m}$, for simplicity.

The number of grid points is $N = 81$, their spacing $h = 10$ km except for the last 10 points at either end, where the grid spacing is increased to 50 km. Hence, the distance between the first and last points measures 1600 km with 650 km normal sections on either side in model 1 and with 800 km for each of the half-sheets in model 2. The linear system has been solved with 12 off-diagonals to either side of the diagonal. Five to ten iterations were needed to determine the respective field quantity with a relative numerical accuracy of 10^{-4} .

Noting that the zero-wavenumber response of the uniform substructure with skin-depth p^+ is $C^+ = p^+ / 2(1 - i)$, or here $150(1 - i)\sqrt{T}$ km, when the period $T = 2\pi/\omega$ is measured in hours, the normal sections should have the required width for periods up to a few hours. The grid-spacing parameter is $\eta_n = 0.01f$ for $\tau = 1000$ S and $0.1f$ for $10\,000$ S with the frequency $f = 1/T$ in c.p.h. This should be adequate for frequencies up to a few cycles per hour, when the condition $h \ll |C^+|$ is also satisfied.

The degree of induction in uniform thin sheets versus induction in the substructure is controlled by the inductive coupling parameter

$$\eta_n = \omega\mu_0\tau_n \Re(C^+)$$

with $\eta_n = 0.003\sqrt{f}$ for $\tau_n = 10$ S and $3\sqrt{f}$ for $\tau_n = 10\,000$ S. Hence, for periods around 1 hr the normal induction currents flow in the substructure on the continental side and mostly in the thin sheet on the oceanic side. The following tests are for frequencies between 0.1 and 100 c.p.h. and assume quasi-uniform source fields unless stated otherwise. Fig. 3 shows the resulting anomalous fields in all components, illustrating their behaviour near the selected test points.

The first test concerns the compatibility of solutions, when the integral equations are solved either for the anomalous current or the anomalous electric field. Table 1 presents the complementary solutions for model 1. Listed values are the normalized tangential electric fields for both polarizations at sensitive grid-points (Fig. 3). For E -polarization the selected point lies in the centre of the conducting slab, where E_x goes through a minimum. For B -polarization two points are chosen, 10 km to either side of the boundary of the slab, where E_y should change discontinuously by a factor of 1000:10. Since the anomalous field is here almost in-phase with the normal field, only real parts of the ratios are quoted.

Table 2 contains the same comparison for model 2, using

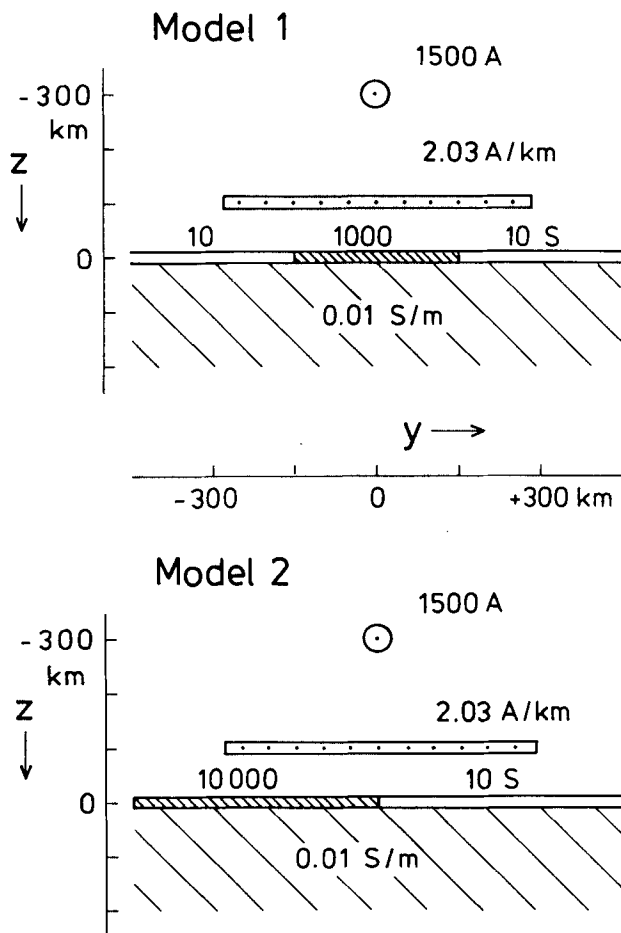


Figure 2. Test models with positions of the line and band currents, when non-uniform sources are studied (Section 6).

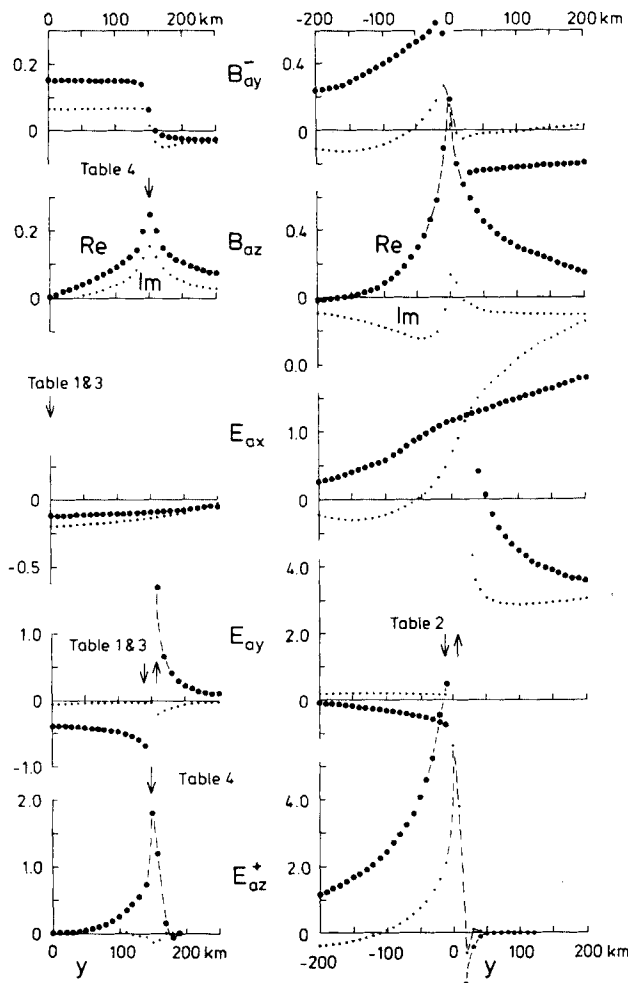


Figure 3. Anomalous field components for model 1 (left) and model 2 (right) for induction by quasi-uniform sources in E - and B -polarization at 1 c.p.h. The magnetic components are normalized with respect to B_{ny}^- , the electric components with respect to E_{nx} and E_{ny} , respectively. Re (large dots) and Im (small dots): real and imaginary parts of ratios B_{ay}^-/B_{ny}^- etc. Boundary points are $y = 150$ km (model 1) and $y = 0$ km (model 2). The influx of in-phase currents from the substructure into the sheet occurs where $Re(E_{az}^+)$ is positive and vice versa. Discontinuities and singularities are smoothed out in the numerical solution.

for B -polarizations again two points at 10 km distance from the 'coastline'. In addition the solutions of both polarizations are tested at the last grid point against their asymptotic

values at infinity. Note that with $\eta_n = 10$ the grid spacing is definitely too coarse on the oceanic half plate for 100 c.p.h. In addition, the penetration depth $\mathcal{R}_e(C^+) = 15$ km into the substructure at this frequency hardly exceeds the grid-point spacing.

Price (1949) suggested that the solution for the sheet current is the preferable one at low frequencies, when self-induction is small, i.e. when in E -polarization E_{ax} disappears and j_{ax} assumes its static value $\tau_n E_{nx}$. At high frequencies, in contrast, the solution for the electric field should be sought, merging into its variable 1-D local value. The test demonstrates that a wide overlap of compatible solutions exists, even close to critical points of discontinuous changes. The same overlap applies to their correct asymptotic behaviour in the case of transition anomalies. It should be noted, however, that the solutions which involve convolutions with derivatives are systematically closer to the asymptotic values. Tests with more grid points support the impression that these solutions are indeed superior. Otherwise the greatest discrepancies are found at high frequencies, as to be expected.

The second test examines the influence of grid-point spacing. Suppose that in E -polarization eq. (35) has been solved for j_{ax} and that E_{ax} has been derived from it with eq. (34). Numerical differentiation of E_{ax} with respect to y yields B_{az} according to eq. (4) and thereby in $(K + L_{TE}) * B_{az}$ (eqs 23 and 33) a second solution j_{ax}^* for testing the grid-point spacing. The degree of agreement indicates how well the convolution integrals with either even (S^+) or odd (K, L) kernel functions are approximated by sums and the derivatives of E_{ax} by finite differences. In the same way the solutions for E_{ay} from eq. (37) can be tested with $E_{az}^+ = -(\partial j_{ay}/\partial y)/\sigma^+$ and $E_{ay}^* = L_{TM} * E_{az}^+$, obtained from eqns (3), (22) and the Price equation.

Table 3 presents the results, using the same test points as in Table 1. For E -polarization discrepancies of less than 1 per cent verify the cited rules for adequate grid-point distances except at the lowest frequency, when j_{ax}/j_{nx} is too close to its limiting static value $\tau_n/\tau_n = 99$. The range of the numerical solution is then not large enough for a correct reconstruction of B_{ay}^- from B_{az} by convolution with K . The entries for B -polarization show the expected tendency that discrepancies increase with frequency. Their substantial size at all frequencies reflects the problematic derivation of E_{ay}^* from E_{az}^+ near to its logarithmic boundary singularity, where a much finer grid-spacing would be needed (cf. Fig. 3, bottom).

In a third test, numerical solutions are compared with

Table 1. Compatibility test of solutions, model 1.

f (cph)	E_x/E_{nx} E -Pol.				$Re(E_y/E_{ny})$ B -Pol.			
	$y = 0$ km		$y = 140$ km		$y = 160$ km			
	Eq. (35)	Eq. (36)	Eq. (37)	(38)	Eq. (37)	(38)		
0.10	0.9911 - 0.0317i	0.9947 - 0.0312i	2.866	2.818	0.3553	0.3551		
0.32	9694	787	9723	809	2.820	2.790	3502	3515
1.00	8969	1725	8972	1741	2.737	2.701	3388	3401
3.16	7082	2824	7090	2827	2.529	2.481	3111	3102
10.0	4365	2766	4338	2803	2.152	2.123	2563	2588
31.6	2644	1860	2580	1869	1.790	1.766	1997	2017
100.	1597	1238	1523	1230	1.455	1.472	1432	1477

Table 2. Compatibility test of solutions, model 2.

<i>f</i> (cph)	E_y/E_{ny} B-Pol.							
	$y = -10$ km				$y = +10$ km			
	Eq. (37)		Eq. (38)		Eq. (37)		Eq. (38)	
0.10	0.2176 + 0.0519i		0.2165 + 0.0486i		14.83 +	3.61i		14.50 + 3.34i
0.32	2602	750	2544	750	17.79	5.31	17.43	5.22
1.00	3224	1042	3227	1044	22.18	7.63	21.81	7.51
3.16	4089	1378	4089	1378	28.49	10.74	27.97	10.55
10.0	5206	1711	5216	1715	37.20	15.04	36.52	14.74
31.6	6622	1952	6610	1942	49.55	21.24	48.36	26.77
100.	8177	1909	8154	1848	66.91	30.29	64.83	30.20

<i>f</i> (cph)	E_{ax}/E_{nx} E-Pol.				E_{ax}/E_{nx} & E_{ay}/E_{ny}	
	$y = 800$ km				$y \rightarrow +\infty$	
	Eq. (35)		Eq. (36)			
0.10 cph	1.67 + 0.91i		1.92 + 0.96i		2.05 + 1.04i	
0.32	2.37	1.81	2.65	1.76	2.86	1.85
1.00	3.81	3.43	4.03	3.22	4.31	3.29
3.16	6.43	6.24	6.58	5.77	6.88	5.81
10.0	11.05	11.52	11.12	10.20	11.46	10.24
31.6	19.28	21.84	19.79	17.97	19.59	17.93
100.	34.36	42.23	33.72	31.68	34.01	30.96

<i>f</i> (cph)	E_{ay}/E_{ny} B-Pol.				E_{ax}/E_{nx} & E_{ay}/E_{ny}	
	$y = 800$ km				$y \rightarrow +\infty$	
	Eq. (37)		Eq. (38)			
0.10 cph	2.04 + 0.84i		2.10 + 0.99i		2.05 + 1.04i	
0.32	2.73	1.58	2.86	1.81	2.86	1.85
1.00	4.13	2.93	4.30	3.29	4.31	3.29
3.16	6.49	4.92	6.88	5.82	6.88	5.81
10.0	10.56	8.11	11.45	10.20	11.46	10.24
31.6	17.24	13.02	19.51	17.82	19.59	17.93
100.	28.49	20.13	33.54	30.47	34.01	30.96

analytical solutions. Weidelt (1971) gives such a solution for transition models in *E*-polarization. His model consists of two uniform half sheets above a substructure which is non-conducting down to a certain depth and then perfectly conducting. Fig. 4 presents a comparison of solutions for the magnetic field, utilizing in the numerical solution the analytical expressions of eq. (32) for the convolution kernels L_{TE} and S^+ . It should be noted that the discontinuous change of j_{ax} at the boundary of the two half sheets implies corresponding discontinuities of B_{ay} and B'_{ay} , while B_{az} at this point has a logarithmic singularity. The numerical solutions naturally can reproduce these discontinuities and singularities only in a smoothed fashion, the degree of

approximation depending on the chosen grid-point distance. Unsuccessful tests have been made with more grid-points in order to improve the agreement for the out-of-phase part of B_{az} on the oceanic half sheet. These and other minor discrepancies remain unexplained.

Bailey (1977) presents an analytical solution of the same problem in *B*-polarization. He allows necessarily for a substructure of finite conductivity (assumed to be uniform), overlain now by only one half sheet which is perfectly conducting. The finite conductances of model 2 are sufficiently extreme to attempt a comparison. As evident from Fig. 5 this model can reproduce Bailey's results quite well. The field components which are compared are the

Table 3. Grid-point spacing test, model 1.

<i>f</i> (cph)	$y = 0$ km		Eq. (35) E-Pol.		$y = 160$ km		Eq. (38) B-Pol.	
	j_{az}/j_{nx}		j^*_{ax}/j_{nx}		E_{ay}/E_{ny}		E^*_{ay}/E_{ny}	
0.10	98.11 -	3.17i	95.88 -	1.74i	1.818 -	0.031i	1.204 -	0.022i
0.32	95.94	7.87	94.05	6.87	1.790	90	1.184	67
1.00	88.70	17.25	88.32	16.74	1.702	222	1.119	167
3.16	69.83	28.24	70.44	28.30	1.481	376	0.952	282
10.0	42.65	27.66	42.31	27.48	1.123	465	0.684	347
31.6	25.44	18.60	25.38	18.55	0.766	433	0.420	317
100.	14.97	12.38	14.84	12.29	0.472	352	0.275	159

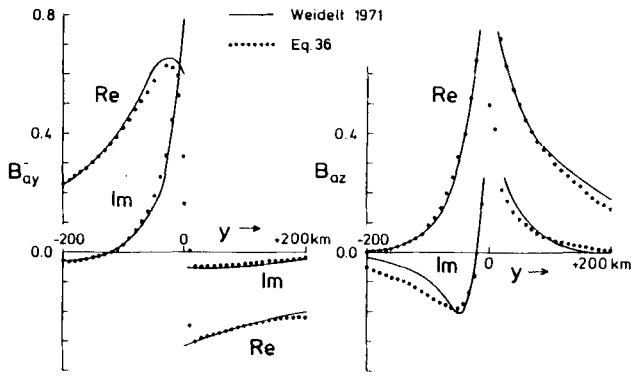


Figure 4. Comparison of Weidelt's analytic solution (1971, Fig. 6) with the numerical solution of eq. (36), using 81 grid points over a range of 1600 km. In the displayed central section the grid-point spacing is 10 km. The thin-sheet model has half sheets of 1600 S ($y < 0$) and 400 S ($y > 0$), meeting at $y = 0$. The substructure is non-conducting down to 200 km depth and then perfectly conducting. Induction is by a quasi-uniform source field in E -polarization at 1 c.p.h. At the boundary line B_{ay} changes discontinuously and B_{az} is singular in response to a discontinuous change of j_{ax} . Unresolved major discrepancies appear on the oceanic half sheet for $\Im(B_{az})$ and on the continental half sheet for $\Re(B_{az})$, both at some distance from $y = 0$. The anomalous field is normalized to B_{ny} .

magnetic field B_x^+ on the underside of the perfectly conducting half sheet, here also the vertical electric field E_z^+ which is responsible for the influx of deep induction currents into the sheet. In addition, E_y is shown for the top of the uncovered part of the substructure. Numerical and analytical solutions disagree most in the out-of-phase part of B_x^+ and in the in-phase part of E_z^+ . This is not unexpected because the finite conductance of the oceanic sheet in model 2 limits the influx of currents from below and increases the overall phase of the sheet currents. An improved fit can be obtained by increasing the conductance ratio of the two sheets to $10^5:1$.

Bailey's model has been extended by Nicoll & Weaver (1977) by assuming a substructure which is terminated at a certain depth by a perfect conductor. If this depth is small against the skin depth of the matter between the thin sheet and perfect conductor, then the inland field E_y and most notably the imaginary part of B_x^+ depend strongly on the depth of the perfect conductor, which has been reproduced numerically to the extent of Bailey's results. Raval, Weaver & Dawson (1981), in considering the E -polarization case of Bailey's model, provide a further analytical solution for testing, supplementing the test with Weidelt's model. However, the assumption of infinite conductivity has even more severe consequences in E -polarization, since E_x drops to zero when approaching the coastline from the continent. Their tabulated numerical results on p. 122 have been confirmed, when the conductance of the well-conducting half sheet is given the highest permissible value for the chosen grid-point spacing.

The test of numerical solutions is more difficult when the source field is non-uniform. The work of Peltier & Hermance (1971) provides the possibility to verify the result for the normal field, when the induction is by a Gaussian jet above a layered structure. For the anomalous field, testing is

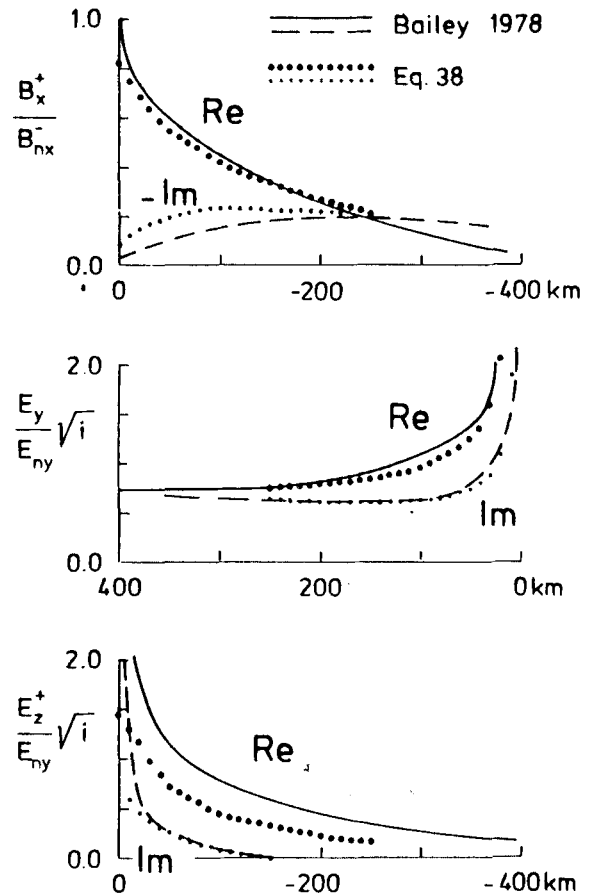


Figure 5. Comparison of Bailey's analytical solution (1977, Fig. 2) with the numerical solution of eq. (38), using the same arrangement of grid points as in Fig. 4. Bailey's model has a perfectly conducting half sheet in $y < 0$ above a uniform half-space (here with 0.01 S m^{-1}). The numerical solutions are for model 2, the induction is by a quasi-uniform source field in B -polarization at 1 c.p.h. (Top) the magnetic field at the underside of the perfectly conducting half sheet; (centre) the tangential electric field at the surface of the uncovered part of the half-space (in Bailey's model); (bottom) the vertical electric field at the top of the half-space beneath the perfectly conducting half sheet, demonstrating the influx of currents from below. The use of finite thin-sheet conductances in model 2 accounts at least partially for the observed discrepancies, most notably in $\Re(E_z^+)$.

restricted at present to a comparison with numerical solutions by others. Agarwal & Weaver (1990) consider the induction of a Gaussian jet above a coastline. Actually their modelling is in three dimensions, but it includes a 2-D case in their model 2. For the chosen frequency of 1 c.p.d. the induction is so weak, however, that even for the oceanic section the normal internal field reaches only one-fifth of the external field and the superimposed anomalous coast effect is hardly visible at all. This limits a detailed comparison and restricts the test to total field ratios at one selected point and three periods as listed in Table 3(b) of the quoted reference. They have been reproduced, at least to the one or two decimals which the authors supply.

A concluding fourth test is designed to study the principal limitation of a thin-sheet approximation. For this purpose a finite thickness d of the top layer is assumed. Setting

$d = 5$ km implies for model 1 conductivities of 0.2 S m^{-1} and 0.002 S m^{-1} for the anomalous and normal sections, respectively. Using finite differences, the 2-D diffusion equation for the anomalous field is solved numerically within the anomalous depth range $[0, d]$. At its upper and lower boundaries the finite-difference solution is combined with eqs (22) and (23) to satisfy conditions at infinity.

The comparison with thin-sheet models is restricted to the most sensitive components with respect to finite thickness which are B_{az} and E_{az} . The chosen point is on the boundary of the conducting slab, where these components go through singularities. They are smoothed in both solutions in similar ways and thus should be comparable. The entries in Table 4 demonstrate the generally observed tendency that the ignored finite depth of induction currents in the thin-sheet approximation exaggerates the extrema of the anomalous vertical fields. Fig. 6 shows how the total toroidal fields for E - and B -polarization would change with depth, if the thin sheets were given a finite thickness. Even though both conditions for a thin-sheet approximation are clearly violated at 100 c.p.h. as pointed out above, the mean fields in the top layer are well represented by the indicated thin-sheet solutions. Therefore it is not surprising that the tests have not yielded any deficiencies up to 100 c.p.h., except for E_{az} in critically close distance to its boundary singularity.

Finally, the numerical solutions are compared with the solution of integral equations (39) and (43), based on Green's theorem. Naturally this test is limited to model 1 with a bounded anomalous range. Table 5 contains for one frequency the respective continuous quantities in each polarization. The selected field points are the central point with maximum deviation from the normal value and three boundary points, when E_x and j_x undergo their strongest change with distance.

Matching results are obtained for E -polarization, but substantial discrepancies appear in B -polarizations. They reflect the already discussed problematic situation, when the influx of currents into the well-conducting part of the thin sheet is strong and Green's function G_{TM} close to its limiting static value. The adopted grid-point spacing of 10 km is much too coarse in comparison with the scaling, which τ_n/σ^1 provides with 1 km, and good agreement is obtained only by lowering σ^1 two orders of magnitude. Experiments with finer grid-point spacings could not resolve the inconsistency of solutions. Those for eqs (37) and (38) proved to be quite invariant, while no stable solution emerged for eq. (43) down to a minimum spacing of 1 km.

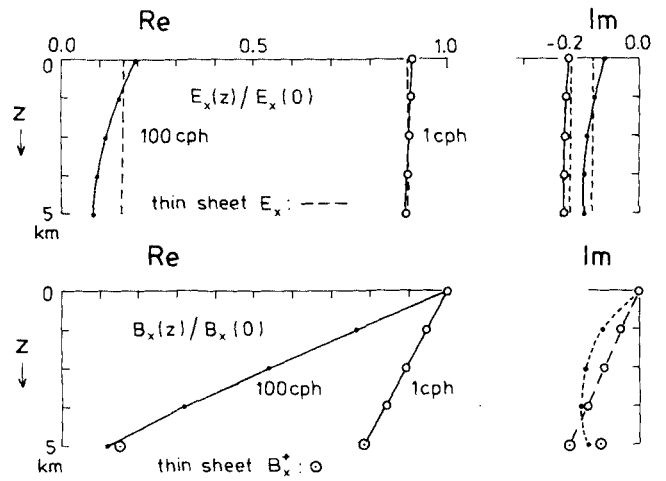


Figure 6. Total fields E_x for E -polarization and B_x for B -polarization as functions of depth for model 1 at grid point $y = 0$, derived from model calculations with a finite thickness of the top layer of 5 km with 0.20 S m^{-1} . It is underlain by a uniform conductor of 0.01 S m^{-1} . At 1 c.p.h. and a skin depth of 67 km the change of E_x between top and bottom is less than 2 per cent while B_x decreases more or less linearly with depth, implying a correspondingly almost constant E_y . The thin-sheet approximation is justified and yields solutions which are in near perfect agreement. At 100 c.p.h. and a skin depth of 6.7 km, the effect of finite thickness becomes visible in a substantial attenuation of E_x and in a slight curvature in the decrease of B_x . The thin-sheet approximation still provides acceptable approximations for E_x within the sheet and for B_x^1 at the bottom.

7 TRANSFER FUNCTIONS

The surface field of models has to be normalized to yield theoretical transfer or response functions for a comparison with observations. In the case of quasi-uniform sources the normalization is straightforward: transfer functions relate the tangential electric field and the magnetic field in all components at a given site to the tangential magnetic field at infinity, or at some chosen reference site, or at the site of observation. For non-uniform sources the concept of transfer functions is practicable only when time-independent linear relations exist between the external field components at different sites.

In the 2-D case relevant here, let y_0 denote the position of a reference site and let $B_{cy}(\omega, y_0)$ be the external source field at that site for E -polarization. Then the external field of any other site should be derivable from a source transfer

Table 4. Test of thin-sheet approximation for point $y = 150$ km, model 1.

f (cph)	B_{az}/B_{ny}		E -Pol.		E_{az}^+/E_{ny} km		B -Pol.	
	thin sheet	finite thickness	thin sheet	finite thickness	thin sheet	finite thickness	thin sheet	finite thickness
0.10	0.077 + 0.071	0.070 + 0.066i	1.920 - 0.021i	1.390 - 0.018i	1.920	63	1.375	49
0.32	140	113	129	109	1.901	63	1.375	49
1.00	247	156	236	149	1.840	158	1.328	121
3.16	392	156	358	144	1.678	284	1.206	218
10.0	506	96	474	90	1.400	373	0.994	287
31.6	560	05	527	+13	1.092	384	0.757	298
100.	497	-137	484	-90	0.798	363	0.531	283

Table 5. Compatibility test of solutions of integral equations with response functions for the substructure (S' , N) and with Green's functions for the total normal structure (G_{TF} , G_{TM}), model 1.

y (km)	E_x/E_{nz}		E -Pol.	
	Eq. (36)		Eq. (39)	
0	0.8972	- 0.1725i	0.8989	- 0.1679i
140	9134	1265	9131	1265
150	9163	1138	9160	1139
160	9192	1010	9189	1012

y (km)	j_y/j_{ny}		B -Pol.	
	$\sigma^+ = 0.01$ S/m		$\sigma^+ = 0.0001$ S/m	
	Eq. (38)	Eq. (43)	Eq. (38)	Eq. (43)
0	59.9 - 5.5 i	27.9 - 1.5 i	2.908 - 0.014 i	2.855 - 0.019 i
140	25.9 2.1	16.2 0.62	2.208 11	2.1549 14
150	5.00 0.40	3.35 0.12	2.001 10	1.995 13
160	1.77 0.14	1.42 0.05	1.810 9	1.770 11

function α defined by $B_{cy}(\omega, y) = \alpha(\omega, y | y_0)B_{cy}(\omega, y_0)$. Since empirical responses are estimated from observations within one or more time segments of finite length, the stated relationship need exist only at certain times, for example during daylight hours. During those hours it is expressed by time-independent cross-covariances, connecting B_{cy} at y and y_0 in the time domain.

Two special cases may be useful to clarify the condition imposed on the source. Suppose the source function α is real and independent of frequency. Then the source field is stationary, for example the field of a line current jet of variable strength but fixed position during all analysed time segments. If in contrast $\alpha = \exp[ik_y(y - y_0)]$ is complex and sinusoidal, then the source field travels with constant speed ω/k_y , in the negative y -direction, as, for example, the field of diurnal variations which move 15 degrees per hour westwards.

Once a linear relation in the above sense has been established, eqs (9) and (10) show that the normal electric and internal magnetic fields are also linearly derivable from B_{cy} , even though now convolutions of inductive responses with source functions are involved and the normal fields at a given site generally are related to B_{cy} at *all* sites. The same applies to the anomalous field and thereby to the total field, as evident from the linearity of the integral equations with regard to E_{ax} and j_{ax} .

In this way any of the field components can be normalized to the source field, the normal field or even the total field at a fixed reference site by transfer functions. As for quasi-uniform sources, a convenient choice for normalization is the tangential magnetic field, defining generalized transfer functions for the electric and magnetic field in reference to $B_{cy}(\omega, y_0)$, $B_m(\omega, y_0)$, $B_y(\omega, y_0)$ or even locally to $B_y(\omega, y)$, but then only for E_x and B_z . The last two options allow direct empirical estimates from observations.

8 STATIONARY AND TRAVELLING NON-UNIFORM SOURCE FIELDS

Stationary source fields are split into two parts: a quasi-uniform 'background' field B_{cy}^0 and a non-uniform 'jet'

field $B_{cy}^j(y)$, which has to be confined to the range of the numerical solutions, i.e. B_{cy}^j must tend to zero within its limits. The two parts are treated separately when deriving the normal field for a given normal structure, utilizing for the background field the fundamental equations (13) and (14). With the notations of Sections 3 and 4 the normal field components are

$$\begin{aligned} E_{nz} &= 2i\omega(C B_{cy}^0 + S * B_{cy}^j), \\ B_{ny} &= 2B_{cy}^0 + B_{cy}^j + P * B_{cy}^j, \\ B_{nz} &= B_{cz}^j - P * B_{cy}^j, \end{aligned} \quad (44)$$

where $B_{cz}^j = -K * B_{cy}^j$. This shows how the background field and the jet field contribute jointly when the anomalous field for E -polarization is derived from the respective integral equation. The same test models of Fig. 2 will be used as in Section 6. Ogunade (1995) discusses results with more realistic earth models.

The first modelling example simulates the induction by daytime fluctuations in equatorial regions. In the vicinity of the dip equator they undergo a strong electrojet enhancement over their nearly uniform amplitudes in adjacent low latitudes. The chosen frequency is 1 c.p.h. The ionospheric jet will be approximated either by a line current of fluctuating strength I_x at height H above the line of zero dip $y=0$ or, more realistically, by a band current of the sheet current density j_x^j at height h and of width $2w$. The band current is symmetrical with regard to the line of zero dip, extending from $y = -w$ to $y = +w$. Both currents flow in the negative x -direction at zero phase (Fig. 2).

The respective heights are chosen in such a way that the extrema of B_{cz}^j occur at the same distance $y = \pm H$. Line currents and band currents are in this sense equivalent, when $H^2 = h^2 + w^2$ (Kertz 1954). Current strength and current density are set to produce a horizontal field of 1 nT at $y = 0$. Source parameters are $H = 300$ km and $h = 100$ km, yielding $w = 283$ km for an equivalent band current.

Figure 7 shows the resulting source fields, derived from

$$B_{cy}^0 = \frac{\mu_0}{2\pi} I_x \frac{H}{H^2 + y^2}, \quad B_{cz}^j = -\frac{\mu_0}{2\pi} I_x \frac{y}{H^2 + y^2}$$

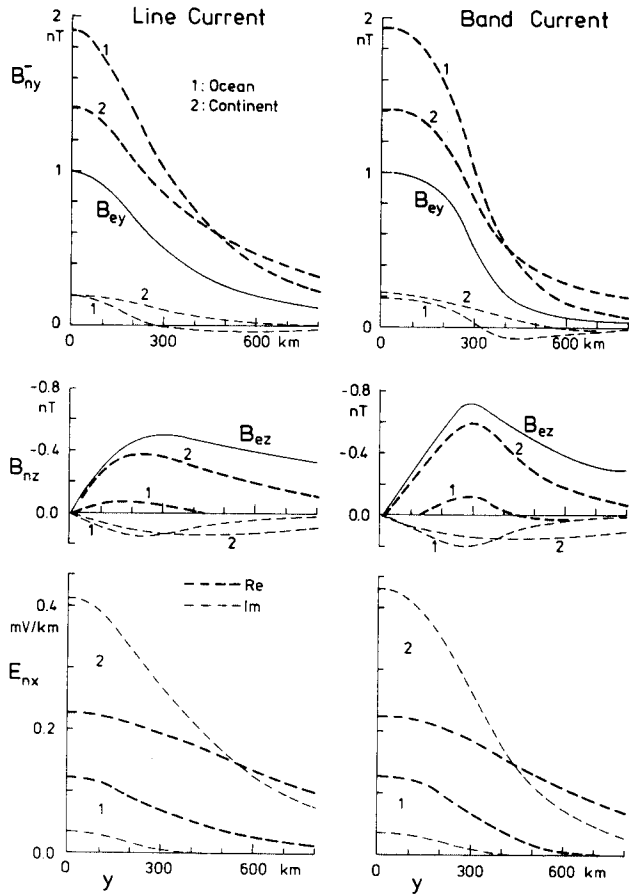


Figure 7. Normal field components for non-uniform stationary jet sources at 1 c.p.h. (cf. Fig. 2 for source position and strength). Zero phase refers to currents in the negative x -direction. The resulting purely in-phase source field components B_{ey} and B_{ez} are shown together with those of the normal field, when the normal internal parts are added. Two sets of normal field components are displayed, one for an oceanic thin sheet of 10 000 S and the second for a continental thin sheet of 10 S. In the oceanic model, induction is close to its upper limit, doubling the horizontal and cancelling the vertical in-phase source field. Out-of-phase fields are negligible. In the continental model, induction is far below this limit and substantial out-of-phase fields occur. However, at great distance B_{ey} is more than doubled by induction and B_{ez} greatly reduced (cf. text for discussion of E_{nx}).

for the line current and from

$$B_{ey}^j = \frac{\mu_0}{2\pi} j_x^j [\arctan(u_+/h) - \arctan(u_-/h)]$$

$$B_{ez}^j = -\frac{\mu_0}{2\pi} j_x^j \log(\sqrt{u_+^2 + h^2}/\sqrt{u_-^2 + h^2})$$

for the band current: $u_+ = y + w$ and $u_- = y - w$. To obtain $B_{ey} = 1$ nT at $y = 0$ requires $I_s = 10^{-9} 2\pi/\mu_0 H = 1500$ A for the line current and $j_x^j = 10^{-9} \pi/\mu_0 \arctan(w/h) = 2.03$ A km⁻¹ for the band current.

The resulting jet fields in Fig. 7 refer either to a normal 'continental' model with $\tau_n = 10$ S for model 1 or to a

normal 'oceanic' model with $\tau_n = 10\,000$ S for model 2. They exemplify the degree of induction by non-uniform sources, which is controlled by their penetration depth (as measured by the zero-wavenumber C^- response) in relation to the source dimensions (here presented by the height H of the line current).

In the continental model with $C = (124 - 107i)$ km, both scales are of comparable magnitude and the induction is far below its limit for a perfect conductor. Hence, B_{ey} is much smaller and smoother than B_{cy} with a far reaching out-of-phase component. The reduction of the vertical source field by internal currents is only minor. For the oceanic model and $C = (6.7 - 37.4i)$ km, the penetration depth is small against H and the induction is close to the limit of a perfect conductor, implying that the horizontal component is nearly doubled by induction and the vertical component is almost reduced to zero.

Consequently, the normal electric field of the oceanic model follows closely the normal field that yields a nearly constant magnetotelluric ratio E_{nx}/B_{ny} at all sites close to the value produced by a quasi-uniform field. In contrast this ratio is quite variable for the continental model and clearly source-dependent in phase and amplitude. Comparing the resulting normal magnetic fields of the line and band current, the sharp B_{ez}^j -extrema at the boundaries of the band currents are slightly smoothed by induction, notably in the oceanic model. But they are still visible in the normal field. The same applies to the sharp decline of the horizontal band current field at 300 km, preserving the difference between the two source fields in the sum of external and internal parts.

The resulting anomalous fields are shown in Fig. 8. The anomalous field of a quasi-uniform source with $B_{cy} = 1$ nT is added to demonstrate the influence of finite source dimensions. It should be recalled that the relevant C^+ -response for the coupling of the anomalous field with the substructure is $150(1 - i)$ km, and therefore is comparable with source dimensions. This strengthens their influence which consists mainly in the reduction of the in-phase part of the anomalous field components, while the out-of-phase part stays the same or becomes even greater. Hence, the weakened induction by finite source dimensions manifests itself also in substantially increased phases. Otherwise the characteristics of the anomalous field remain essentially unchanged: the B_{ez} -extrema at conductance boundaries, positive B_{ay} -anomalies above well-conducting sections and negative B_{ay} -anomalies where the thin-sheet conductance is low. Now the induction by a travelling source will be considered.

Sources which are periodic in space will in general consist of a mixture of standing and travelling parts. In the frequency-space domain they are expressed in the form of line spectra, each spectral term of amplitude $a(\omega, k_y)$ with $\exp[i(\omega t + k_y y)]$ as the time-distance factor. Standing parts evolve if, at a certain frequency and wavenumber, two terms of the same amplitude, but with opposite signs of k_y , are added. The total normal field is derived by summation over the spectra of the electric and internal magnetic field, which are found as follows: let $C^-(\omega, k)$ be the C^- -response of the normal structure at frequency ω and wavenumber $k = |k_y|$. Then, as seen from eqs (6)–(8), a single spectral source term with $B_{cy}(\omega, y) = a(\omega, k_y) \exp(ik_y y)$ as ground field has

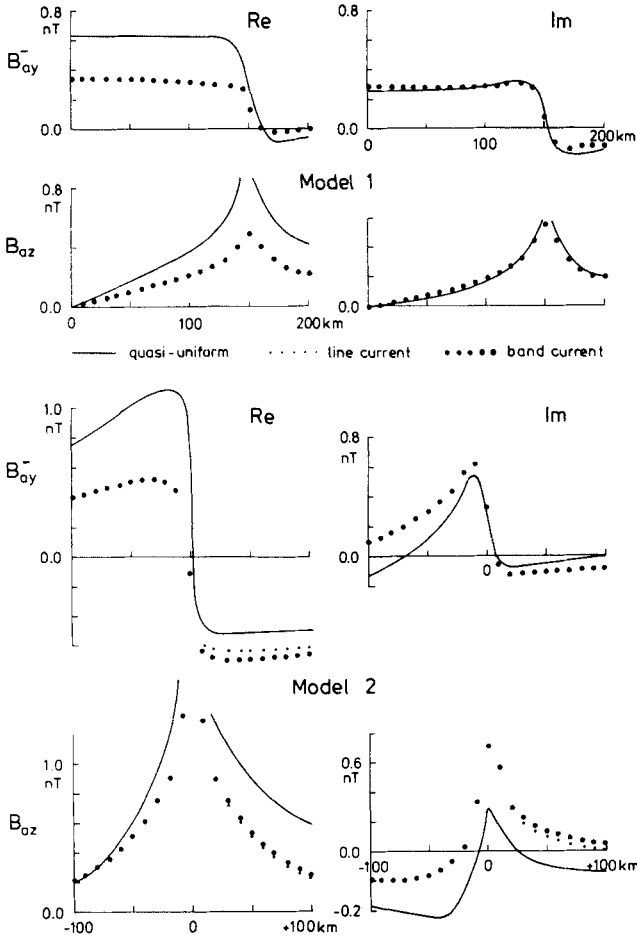


Figure 8. Anomalous magnetic fields for model 1 (top) and model 2 (bottom) at 1 c.p.h. derived with the normal fields E_{nx} of Fig. 7. This figure compares the quasi-uniform source solution for $B_{cy}^0 = 1 \text{ nT}$ with non-uniform source solutions for line and band current jets. Finite source dimensions reduce B_{ay} above well-conducting sections and also the edge anomalies of B_{az} , but only in their real parts which implies a considerable increase of phases. Note that in the coastline model, the decrease in B_{az} towards inland is more rapid for jet sources than for a quasi-uniform source, which reflects the decreasing strength of the inducing field with distance from the coast and jet centre. The out-of-phase part of B_{az} preserves its complicated behaviour, but with an overall upward shift. Line and band current jets of equivalent dimensions (*cf.* text) produce nearly the same anomalous fields. See Fig. 10 for apparent resistivities and phases from local magnetotelluric ratios.

the normal field components

$$\begin{aligned}
 E_{nx} &= i\omega \frac{2C}{1+kC} B_{cy}, \\
 B_{ny}^- &= \frac{2}{1+kC} B_{cy}, \\
 B_{nz} &= \frac{2kC}{1+kC} B_{cz}
 \end{aligned} \quad (45)$$

with $B_{cz} = ik_y/kB_{cy}$. The sum over all spectral constituents provides the normal field for subsequent calculations of the anomalous field. In the case of transition anomalies it has to

be noted that the anomalous field has to merge for $y \rightarrow +\infty$ into an oscillatory difference of two normal solutions. Therefore the numerical convolutions in *both* integral equations (35) and (36) are extended several penetration depths beyond the last grid point, inserting here for the anomalous current density or the anomalous electric field the known difference of their two normal solutions.

The following example refers to the special case of a travelling sinusoidal source as expressed by a single spectral term, here in correspondence to the third time-harmonic of daily variations, moving with the Sun over the Earth's surface. The chosen wavenumber is $k = 6.614 \times 10^{-4} \text{ km}^{-1}$ for a wavelength $\lambda = 2\pi/k$ of 9500 km which is one-third of the circle of latitude at 45° . At frequency $f = 0.125 \text{ c.p.h.}$ this gives the ground field the required speed λf of roughly 1200 km h^{-1} or 15 degrees longitude per hour.

Since daily variations move westwards, the positive y -axis is towards the east and x towards the north, when k_y is positive, and vice versa. The non-uniformity of daily variations in the meridional direction, which is actually more important, must be ignored. For a less restrictive treatment of the Sq induction problem the reader is referred to the publications on spherical earth models already cited, also to the works by Roden (1964), Parker (1968), and Bullard & Parker (1970).

The $C(\omega, k)$ -responses to be used are $C^+ = (457 - 390i) \text{ km}$ for the uniform substructure of $100 \Omega\text{m}$, $C^- = 456 - 390i \text{ km}$ for the normal continental structure ($\tau_n = 10 \text{ S}$), and $C = (78 - 236i) \text{ km}$ for the normal oceanic structure ($\tau_n = 10000 \text{ S}$). All are still far off their limiting values of no induction which is $k^{-1} = 1512 \text{ km}$. The C -response of the third harmonic of daily variation actually observed when observatory data on continents are analysed is $(400 - 300i) \text{ km}$, and is thus quite similar. In any case, source dimensions, as expressed in this example by the reciprocal wavenumber, are about three times larger than penetration depths, while in the previous example of daytime fluctuations under the equatorial electrojet this ratio was two to one. Accordingly a reduced source effect on the anomalous field can be expected.

The external field amplitude is set to $a = 1 \text{ nT}$ which yields from eq. (45) with the quoted response values

$$\begin{aligned}
 E_{nx} &= (97 + 172i) \mu\text{V km}^{-1}, \\
 B_{ny}^- &= (1.48 + 0.29i) \text{ nT}, \\
 B_{nz} &= (0.29 + 0.52i) \text{sgn}(k_y) \text{ nT}
 \end{aligned}$$

for continents and

$$\begin{aligned}
 E_{nx} &= (91 + 46i) \mu\text{V km}^{-1}, \\
 B_{ny}^- &= (1.86 + 0.28i) \text{ nT}, \\
 B_{nz} &= (0.28 + 0.14i) \text{sgn}(k_x) \text{ nT}
 \end{aligned}$$

for oceans. The common distance factor $\exp(ik_y y)$ has been omitted. For a quasi-uniform source ($k^{-1} \gg |C|$) the normal electric fields would have been $102 + 30i \mu\text{V km}^{-1}$ for oceans and $(186 + 185i) \mu\text{V km}^{-1}$ for continents, while B_{ny} is 2 nT and B_{nz} zero in either case. The quoted values demonstrate how the finite source dimensions reduce the size of the secondary field and increase its phase with respect to the primary field.

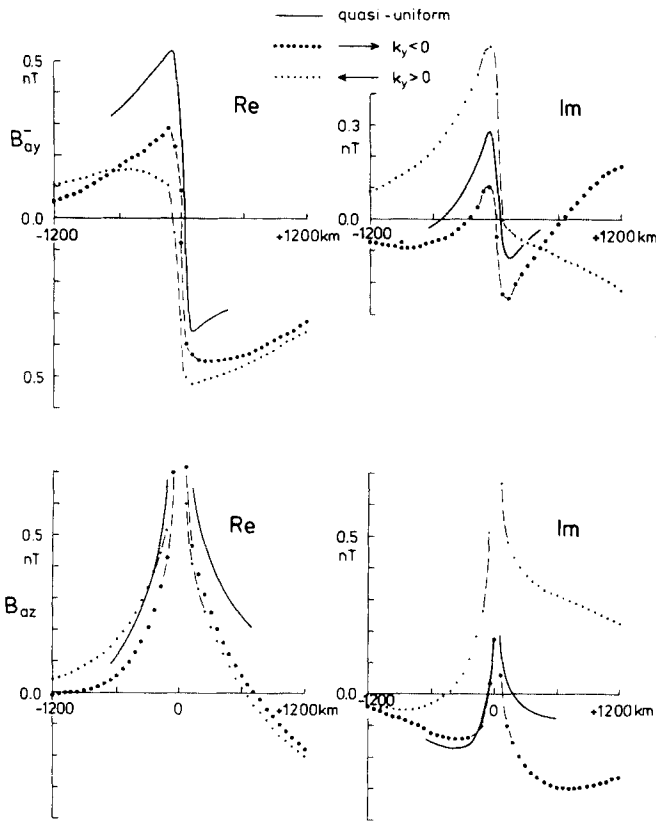


Figure 9. Anomalous magnetic fields for model 2 at 3 c.p.h. and a travelling source. It resembles the motion of the third harmonic of daily variations with the Sun around the Earth. Arrows indicate the travelling direction. *cf.* text for amplitude and phase of the normal field components. Again the quasi-uniform source solution for $B_{cy}^0 = 1 \text{ nT}$ is added for comparison. Note that the displayed distance range is small against the source wavelength of 9500 km, i.e. the source field variations within this range are small: $B_{cy} = 0.7 \text{ nT}$ at $\pm 200 \text{ km}$ versus $B_{cy} = 1 \text{ nT}$ at $y = 0$. But because of the large penetration depth of 400 km, finite source dimensions strongly influence the anomalous field. The in-phase fields are reduced in similar ways as has been observed for stationary jet sources (*cf.* Fig. 8 and text), but the out-of-phase fields are now even more enhanced with characteristic differences in dependence on the direction in which the source travels (*cf.* text for further discussion). Note that away from the coast on the continental side ($y > 0$) the anomalous field starts to merge into the oscillating difference of normal solutions for continents and oceans.

Figure 9 shows the resulting anomalous magnetic fields for model 2, in comparison with the anomalous fields for a quasi-uniform source field. In order to accentuate the source effect, the calculations have been carried out with both signs of k_y . For $k_y > 0$ the source field approaches the coastline from the continent, for $k_y < 0$ from the ocean. It is clearly seen how in the first case the presence of the ocean accelerates the internal field before actually reaching the coast. In the second case the internal field slows down well offshore, adjusting itself still in the ocean to the increased phase on land.

With regard to the electric fields which have been ignored so far, they are not presented here as such, but as local magnetotelluric ratios E_x/B_y^- which would be observed beneath the stationary jet sources discussed in model 2 at

1 c.p.h. Offshore the field on the underside of the oceanic sheet is taken, simulating in the ratio E_x/B_y^+ magnetotelluric sea-bottom observations. Fig. 10 shows the resulting ratios in the form of apparent resistivities $\rho_a = \mu_0/\omega |E_x/B_y|^2$ and phases $\phi = \arg(E_x/B_y)$.

The concentration of oceanic induction currents beginning far offshore lowers $|B_y^+|$ and produces ρ_a -values far in excess of the normal value, here $100 \Omega\text{m}$. This reduction of B_y^+ outweighs the concurrent smooth increase of E_x . Approaching the coastline B_y^+ in its real part changes sign and continues to decrease, causing ρ_a to drop below the normal level, to which it returns slowly on land. The sea-bottom phases, emerging from an offshore minimum, rise sharply near the coast passing 90° , while the continental surface phases do not deviate much from their normal half-space value of 45° . The influence of finite source dimensions on this magnetotelluric coast effect can be described as follows: the weakened induction by jets leads to

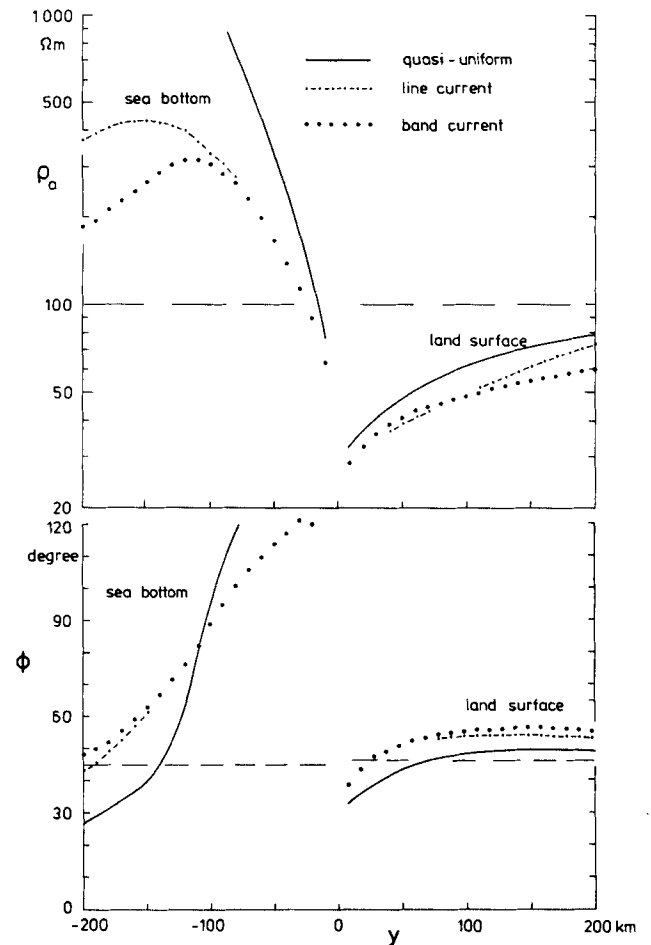


Figure 10. Local total field magnetotelluric ratio, in the form of apparent resistivities and phases, for model 2 at 1 c.p.h. and stationary jet sources. On the oceanic side $y < 0$ apparent resistivities and phases refer to the sea-bottom ratio E_x/B_y^+ , on the continental side $y > 0$ to the surface ratio E_x/B_y^- . Deviations from the normal levels of $100 \Omega\text{m}$ and 45° shown reflect the combined influence of coastlines on E_x and B_y . Large deviations occur for ρ_a on the oceanic side, in particular when the source is quasi-uniform. On the continent ρ_a and ϕ return to their normal levels within the shown distance range (*cf.* text for further discussion).

a smoother sea-bottom field B_v^+ and brings thereby ρ_a offshore closer to the normal level. The same applies to the magnetotelluric phase.

Correspondingly, a generalized $Z:H$ response can be defined from the local B_z/B_v ratio. This geomagnetic deep sounding response for layered structures utilizes the non-uniformity of the sources, which must be known, to determine C . As readily seen from eq. (45), B_{nz}/B_{ny} for such normal structures equals $C(\omega, k)ik_v$, if an oscillatory source field at a given frequency is adequately described by a single spectral term of wavenumber k . In the general case the source non-uniformity may be approximated by locally derived derivatives of the tangential magnetic field, replacing in the 2-D case ik_v by $(\partial B_{ny}/\partial y)/B_{ny}$.

The following modelling example concerns the influence of coastlines on geomagnetic deep sounding studies with diurnal variations, here with its third harmonic and thus a well-defined wavenumber as specified above and with the anomalous field of Fig. 9. Again sea-floor observations B_v^+ will be inserted offshore and land-based observations B_v^- inland, yielding

$$C^\pm = (B_z/B_v^\pm)/ik_v$$

as the locally determined C -responses. Noting that at 3 c.p.d. the continental thin sheet has hardly any effect, the undisturbed C -responses on either side of the coast are about the same and given by $C^\pm(\omega, k)$ for the underlying half-space as quoted above. Fig. 11 demonstrates to which

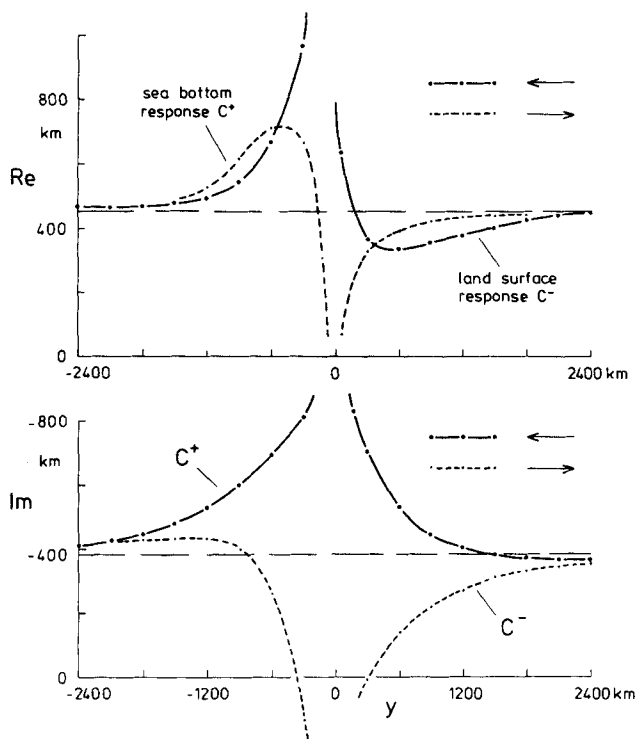


Figure 11. Local total field geomagnetic $Z:H$ ratio, in the form of C -responses for model 2 at 3 c.p.d. and a travelling Sq source. The resulting coast effect on the response is distinctly non-symmetric with respect to the coastline at $y = 0$ and depends on the indicated direction of travel. It extends in either case to distances of several substructure penetration depths into the continent and ocean (*cf.* text for further discussion).

distances from the coast the $Z:H$ response deviates from the normal level thus defined.

These distances depend on the direction of propagation, in correspondence to the directional dependence of the anomalous field as outlined above. If daily variations approach a coastline from the continent (such as the Atlantic coast from the European mainland), then the coast effect on the real part of the $Z:H$ ratio and thereby the imaginary part of C^+ extends to, say, 1600 km out at sea, but only 800 km inland. This is reversed, when the westward travelling source approaches a coastline from the ocean (such as the Atlantic coast on the American side), while the real part of C^+ shows a more complicated behaviour. The quoted distances are to be seen in relation to the C^+ response of the substructure at the relevant period and wavenumber, allowing a generalization to more realistic earth models and other Sq harmonics.

9 CONCLUDING REMARKS

The numerical procedures for thin-sheet modelling in two dimensions described above combine the advantage of solving integral equations with the possibility of including transition anomalies. In this respect a correspondence exists to the integral equation method of Dawson & Weaver (1979). Their equations generate, however, the total field directly from a given source field rather than in two computational steps, first, the normal field from the source field and then secondly the anomalous field from the normal field, as done in this paper. In this respect an analogy exists to the integral equation method of Vasseur & Weidelt (1977).

A special advantage of the method presented here lies in the possibility of self-correction with two complementary solutions. Countless conceptual and programming errors have been found this way. Thin sheets in general offer the unique opportunity of analytical solutions for testing, not only in two dimensions as used here but also in three dimensions (Price 1949; Ashour 1974).

The thin-sheet inverse problem for interpreting data can be formulated in two ways: to find the anomalous conductance for a given normal structure, or vice versa to find the normal substructure response for a known surface conductance. For the first problem explicit expressions are possible in both polarizations for the unknown anomalous conductance. An application in three dimensions has been performed by Singer *et al.* (1984). The second problem requires an iterative approach, since the inductive coupling with the substructure involves both the normal and the anomalous fields. An example is the investigation of the crustal structure beneath the Rhein Graben, using the fairly well-known conductance of the Rhein Graben sediments (Winter 1974).

An extension to three dimensions of the modelling technique presented here may be feasible. It is not difficult to formulate the response function for 3-D fields which would generate the normal field from a given source field and which would provide the coupling of the anomalous field to the substructure. It is also not difficult to generalize the conditions at the upper surface of the thin sheet because here only the poloidal parts of the now two modes of the anomalous magnetic field are present. In contrast the

coupling conditions at the underside of the sheet involve anomalous tangential fields which are of dual origin with different responses for their tangential electric and their tangential magnetic modes.

ACKNOWLEDGMENTS

I am grateful to Dr Andreas Junge for reading the manuscript in various versions, to Dr John Weaver and Dr Peter Weidelt for their illuminating reviews and to Professor Samuel Ogunade who inspired my renewed interest in the subject with his admirable observations in Nigeria, close to the coast and not far from the equatorial electrojet.

REFERENCES

- Agarwal, A.K. & Weaver, J.T., 1990. A theoretical study of induction by an electrojet over a coastline for Sq and substorm periods, *Phys. Earth planet. Inter.*, **61**, 165–181.
- Ashour, A.A., 1974. Exact solutions for certain axisymmetric problems of induction in thin nonuniform sheets, *J. geophys. Res.*, **79**, 2479–2486.
- Bailey, R.C., 1977. Electromagnetic induction over the edge of a perfectly conducting ocean: the *H*-polarization case, *Geophys. J. R. astr. Soc.*, **48**, 385–392.
- Berdichevsky, M.N. & Zhdanov, M.S., 1984. *Advanced Theory of Deep Geomagnetic Soundings*, Elsevier, Amsterdam.
- Bullard, E.C. & Parker, R.L., 1970. Electromagnetic induction in the oceans, in *The Sea*, Vol. 4, Ch. 18, ed. Maxwell, A.E., John Wiley, New York.
- Dawson, T.W. & Weaver, J.T., 1979. Three-dimensional induction in a non-uniform thin sheet at the surface of a uniformly conducting earth, *Geophys. J. R. astr. Soc.*, **59**, 445–462.
- Dmitriev, V.I., 1969. The magnetotelluric field in thin inhomogeneous layers, *Colloq. Comput. Methods Programming Moscow State Univ.*, **13**, 231–236.
- Fainberg, E.B., Kuvshinov, A.V. & Singer, B.Sh., 1990. Electromagnetic induction in a spherical earth with non-uniform oceans and continents in electric contact with the underlying medium—I. Theory, method and example, *Geophys. J. Int.*, **102**, 273–281.
- Hewson-Browne, R.C., 1978. Induction in arbitrarily shaped oceans—III. Oceans of finite conductivity, *Geophys. J. R. astr. Soc.*, **55**, 645–654.
- Hobbs, B.A. & Brignall, A.M.M., 1976. A method for solving general problems of electromagnetic induction in the oceans, *Geophys. J. R. astr. Soc.*, **45**, 527–542.
- Kertz, W., 1954. Modelle für erdmagnetisch induzierte elektrische Ströme im Untergrund, *Nachr. Akad. Wiss. Göttingen Math. Phys. Klasse IIa*, **5**, 101–110.
- McKirdy, D.McA., Weaver, J.T. & Dawson, T.W., 1985. Induction in a thin sheet of variable conductance at the surface of a stratified earth—II. Three-dimensional theory, *Geophys. J. R. astr. Soc.*, **80**, 177–194.
- Nicoll, M.A. & Weaver, J.T., 1977. *H*-polarisation induction over an ocean edge coupled to the mantle by a conducting crust, *Geophys. J. R. astr. Soc.*, **49**, 427–441.
- Ogunade, S.O., 1995. Analysis of geomagnetic variations in Southwestern Nigeria, *Geophys. J. Int.*, **121**, 162–172, this issue.
- Parker, R.L., 1968. Electromagnetic induction in a thin strip, *Geophys. J. R. astr. Soc.*, **14**, 487–495.
- Peltier, W.R. & Hermance, J.F., 1971. Magnetotelluric fields of a gaussian electrojet, *Can. J. Earth Sci.*, **8**, 338–346.
- Price, A.T., 1949. The induction of electric currents in non-uniform thin sheets and shells, *Q. J. Mech. appl. Math.*, **2**, 283–310.
- Ranganayaki, R.P. & Madden, T.R., 1980. Generalized thin sheet analysis in magnetotellurics: an extension of Price's analysis, *Geophys. J. R. astr. Soc.*, **60**, 445–457.
- Raval, U., Weaver, J.T. & Dawson, T.W., 1981. The ocean-coast effect re-examined, *Geophys. J. R. astr. Soc.*, **67**, 115–123.
- Roden, R.B., 1964. The effect of an ocean on magnetic diurnal variations, *Geophys. J. R. astr. Soc.*, **8**, 375–388.
- Schmucker, U., 1970. Anomalies of geomagnetic variations in the Southwestern United States, *Bull. Scripps Inst. Oceanogr.*, **13**, 1–165.
- Schmucker, U., 1971. Interpretation of induction anomalies above non-uniform surface layers, *Geophysics*, **36**, 156–165.
- Schmucker, U., 1986. 2D-modellrechnungen—neue fassung älterer programme, in *Elektromagnetische Tiefenforschung Kolloquium Lerbach*, pp. 5–44, eds Haak, V. & Homilius, J., Niedersächsisches Landesamt für Bodenforschung, Hannover.
- Singer, B.Sh., Dubrovsky, V.G., Fainberg, E.B., Berdichevsky, M.N. & Ithamov, K., 1984. Quasi three-dimensional modelling of magnetotelluric fields in the South-Turanian platform and in the South-Caspian megadepression, *Izv. Akad. Nauk SSR, Phys. Earth*, **1**, 69–81.
- Vasseur, G. & Weidelt, P., 1977. Bimodal electromagnetic induction in non-uniform thin sheets with an application to the northern Pyrenean induction anomaly, *Geophys. J. R. astr. Soc.*, **51**, 669–690.
- Weidelt, P., 1971. The electromagnetic induction in two thin half-sheets, *Z. Geophysik*, **37**, 649–665.
- Winter, R., 1974. A model for the resistivity distribution from geomagnetic depth sounding, in *Approaches to Taphrogenesis*, pp. 369–375, eds Illies, H. & Fuchs, K., E. Schweizerbart'sche Verlagsbuchhdlg. Stuttgart.
- Yegorov, L.V., Chernyak, E.L., Palshin, N.A. & Demidova, T.A., 1983. Numerical thin-sheet modelling of the telluric field distortions by the hybrid techniques. I. Theory and an example for the Baltic Shield, *Phys. Earth planet. Inter.*, **33**, 56–63.
- Zinger, B.Sh. & Fainberg, E.B., 1980. Method for computing electromagnetic fields in the World Ocean, *Geomagn. Aeronomy* (English edition), **20**, 67–69.